Transport of hydrogenic species in crystalline oxides: radiation and electric-field-enhanced diffusion

2002 J. Phys.: Condens. Matter 14 R1143

(http://iopscience.iop.org/0953-8984/14/45/201)

INSTITUTE OF PHYSICS PUBLISHING JOURNAL OF PHYSICS: CONDENSED MATTER

J. Phys.: Condens. Matter **14** (2002) R1143–R1173 PII: S0953-8984(02)23820-5

TOPICAL REVIEW

Transport of hydrogenic species in crystalline oxides: radiation and electric-field-enhanced diffusion

R González and Y Chen[1,2]

Departamento de Física, Escuela Politécnica Superior, Universidad Carlos III, Avda. de la Universidad, 30, 28911 Leganés, Madrid, Spain

Received 6 February 2002, in final form 23 September 2002
Published 1 November 2002
Online at stacks.iop.org/JPhysCM/14/R1143

Abstract

Thermal diffusion of protons, deuterons and tritons forming OH^-, OD^- and OT^- radicals respectively was monitored by infrared absorption measurements in MgO, Al_2O_3, $LiNbO_3$ and TiO_2 single crystals. The electric charge and/or ionic radius is shown to be more important than mass in affecting the diffusion behaviour in these oxides. The influence of selected impurities and crystal orientation on the diffusion parameters was also investigated. Thermal diffusion of protons occupying substitutional anion vacancies (hydride ions) or $[H^-]^+$ centres was studied in thermochemically reduced MgO crystals. Simulations using an *ab initio* Hartree–Fock cluster approach indicate that the mobile defect is more compatible with the H^- ion than with the proton.

Application of even a moderate electric field is very effective in enhancing the $H^+ \leftrightarrow D^+$ exchange in crystals containing hydroxyl ions. In addition, deuterons can be effectively incorporated in crystals with undetectable hydrogen concentrations by applying moderate electric fields at elevated temperatures. The incorporation of deuterons occurs without proton replacement, which indicates the possibility of D^+ (H^+) doping.

Under electron irradiation, otherwise stable hydrogenic species become mobile at temperatures as low as 85 K. Ionizing radiation breaks the O–H bond with exceedingly large cross-sections (10^8 barns at room temperature), which is a strong function of the irradiating temperature. The displacement cross-section of protons is twice that of deuterons. Radiation induced displacement of protons from hydride ions at room temperature is also discussed. Out-diffusion of hydrogen isotopes can be induced in TiO_2 crystals near room temperature by breaking the hydroxyl bond by electron irradiation and subsequently sweeping out hydrogenic species along the *c*-axis by application of an electric field.

[1] This research of Y Chen is an outgrowth of past investigations performed at the Solid State Division of the Oak Ridge National Laboratory from 1965 to 1994.

[2] Present address: US Department of Energy, SC-13, Office of Basic Energy Sciences, Division of Materials Science, Germantown, MD 20874-1290, USA.

0953-8984/02/451143+31$30.00

Contents

1. Introduction

In recent years there has been increasing interest in understanding the fundamental properties of hydrogen impurities in oxide crystals. Hydrogen exists in most as-grown oxide crystals as a ubiquitous impurity that profoundly influences the electronic, mechanical and optical characteristics of these materials, especially for device applications [1–12]. Its influence can be detrimental: in SiO_2 glass fibres an annoying OH peak seriously interferes with optical communications [7, 8]. On the other hand, beneficial effects associated with the presence of hydrogen occur in ZnO, where interstitial hydrogen acts as a source of conductivity [9, 10], and in $LiNbO_3$, where many applications are based on the introduction of hydrogen [11, 12]. These are just a few examples of how the incorporation of hydrogen can change the properties of oxides.

Ceramic oxides are required for several applications in advanced energy systems, sometimes under very stringent operating conditions [13–15]. Of great importance to the use of ceramics in fusion reactors are the problems associated with the presence of high levels of transmutation products induced by high-energy neutrons. The concentration of these products has been calculated for several ceramics [16]. For aluminium oxide, which is the strongest candidate for insulators and RF windows in fusion devices, the four major transmutation products are, in increasing order of concentration, magnesium, hydrogen, carbon and helium [16]. After 1 year of operation, the expected concentration of hydrogen is of the order of several hundred atomic parts per million (appm) [16]. The effects of such a large concentration of hydrogen have not yet been studied, but it can be assumed to significantly modify the electronic, optical and mechanical properties of this oxide.

Hydrogenic species (protons, deuterons and tritons) normally occupy stable configurations in oxide crystals and do not diffuse until several hundred degrees above room temperature [17, 18]. Hydrogen and its isotopes, deuterium and tritium, diffuse much more slowly in insulators than in metals. While some metals are suitable for hydrogen storage applications, the usefulness of ceramics lies precisely in their low-permeability to hydrogen. The characterization of hydrogenic species is important to determine the solubility and diffusivity of hydrogen in these materials. Since the 1970s major efforts have been made to study the diffusion behaviour of hydrogen isotopes in ceramic oxides [19–38].

Under ionizing radiation, such as gamma or electron irradiation, hydrogenic species are displaced readily from cation and anion sites and become highly mobile (referred to as radiation induced diffusion (RID)) [17, 30, 36, 39, 40]. Therefore, the usual diffusion constants for these isotopes cannot be used to predict their behaviour in insulators under ionizing radiation. Because of their mobility, they can be swept in and out of a crystalline material using an applied electric field at temperatures at which this would not be possible by purely thermal means [30, 36].

The purpose of this review article is to provide fundamental information about the current understanding of the interaction of hydrogen with crystalline oxides, which includes (1) knowledge of the hydrogen site preference, (2) the isotopic effect, (3) dependence on crystal orientation, (4) effects of doping with selected impurities and (5) the influence of external conditions such as radiation and electric field. These issues will be illustrated with data from four crystalline oxides, MgO, Al_2O_3, $LiNbO_3$ and TiO_2, with different crystalline structures. Rather than a fully comprehensive presentation of the investigations reported in the literature, for each oxide special emphasis will be placed on those studies which address these topics. We shall first discuss thermal diffusion of protons forming hydroxyl ions in these oxides and the associated isotopic effect. Second, the influence of both crystal orientation and selected impurities on the diffusion parameters will be addressed. Third, in RID experiments the displacement cross-sections for protons and deuterons are determined to be a strong function of the irradiating temperature. Finally, it is demonstrated that the application of a moderate electric field enhances the $H^+ \leftrightarrow D^+$ exchange. Deuterons can be introduced without an exchange process, opening up the possibility of D^+ (H^+) doping.

2. Hydrogen configurations in crystalline oxides

To a greater or lesser extent all oxide crystals contain hydrogen, which enters the lattice during crystal growth. Most of the hydrogen appears in three basic forms or configurations: OH^-, H_2 and $[H^-]^+$. Hydroxyl ions (OH^-) are normally present in all crystalline oxides. In as-grown Al_2O_3 crystals their concentrations range from 10^{15} to 10^{16} cm^{-3}, while in $LiNbO_3$ hydroxyl concentrations can be as high as 10^{18}–10^{19} cm^{-3}. Intermediate concentrations of 10^{16}–10^{17} and 10^{17}–10^{18} cm^{-3} are determined in MgO and TiO_2 crystals respectively. High-pressure hydrogen gas (H_2) has been found to be present in cavities in MgO, resulting in opacity of the crystal [41, 42]. Lastly, hydride ions $[H^-]^+$ substituting for O^{2-} ions have been observed in alkaline-earth oxides after a severe thermochemical reduction (TCR) at elevated temperatures [43]. Next, we will analyse in more detail the hydrogen configurations in MgO, Al_2O_3, $LiNbO_3$ and TiO_2 crystals.

In as-grown MgO single crystals, the two most prominent infrared absorption bands associated with the stretching frequencies of the OH^- radicals occur at 3296 and 3700 cm^{-1}, with their OD^- analogues peaking at 2445 and 2723 cm^{-1} respectively. Previous studies (see [28] and references therein) have established unambiguously the origin of these bands. The 3296 cm^{-1} band has been attributed to a proton *substituting* for an Mg^{2+} ion. The H^+ in

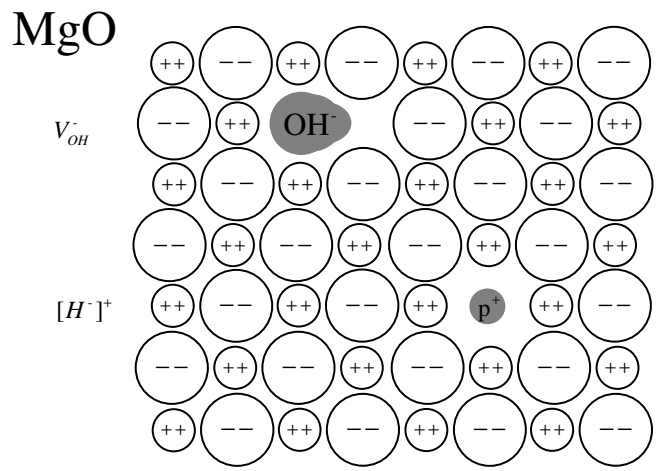

Figure 1. Schematic depiction of the rock-salt crystalline structure of MgO crystals containing V_{OH}^{-} and $[H^{-}]^{+}$ centres.

this site is affected by covalent bonding to one of the six neighbouring oxygen ions and the resulting lattice distortion yields the following linear configuration: OH^{-} [++]O^{2-}, where [++] refers to a Mg^{2+} vacancy (figure 1). This defect is commonly referred to as the V_{OH}^{-} centre. The 3700 cm^{-1} band is due to OH^{-} ions in $Mg(OH)_2$ precipitates. In thermochemically reduced MgO crystals, hydride ions, or $[H^{-}]^{+}$ centres, are formed. An $[H^{-}]^{+}$ ion consists of a *substitutional* proton with two electrons occupying an oxygen vacancy site, and therefore has a net positive charge (figure 1). The fundamental $[H^{-}]^{+}$ ion vibrational frequencies in MgO produce three sharp lines at 1024, 1032 and 1053 cm^{-3} [43].

Infrared absorption bands at 3185, 3233, 3279, 3296 and 3310 cm^{-1} have been identified in α-Al_2O_3 crystals (trigonal crystal structure) and attributed to OH^{-} ions probably perturbed by impurities nearby [26, 37]. Theoretical calculations [26] in conjunction with polarization experiments [26, 37] indicate that the proton occupies an *interstitial* site in the plane formed by the three oxygen atoms of the aluminium oxide molecular unit (basal plane); the orientation of the OH^{-} ion is that of the direction directly away from the centre of the oxygen triangle (figure 2).

In $LiNbO_3$ crystals with a trigonal structure, the broad infrared band arising from the OH^{-} stretching bond is centred at about 3500 cm^{-1}; its exact energy position depends on the stoichiometry, doping impurities or production method [11, 12, 44]. This band is strongly polarized perpendicular to the ferroelectric c-axis [11, 12, 44]. In the models proposed to explain the OH^{-} band, the proton is in an *interstitial* site lying in the oxygen plane perpendicular to the c-axis, and the bond is directed towards one of the six nearest O^{2-} ions (figure 3) [45–47]. Protons only occupy positions 1–4. The longest O–O bonds (positions 5 and 6) are not occupied because the length (336 pm) of the bond is too large [45–47].

TiO_2 (rutile) has a tetragonal structure ($a_0 = 0.4594$ nm and $c_0 = 0.2958$ nm) with large open channels parallel to the c-axis. The predominant hydrogen-containing species in rutile are hydroxyl ions, absorbing at about 3277 cm^{-1} [22, 30, 48], in which the oxygen occupies a regular oxygen ion site, the proton is in an *interstitial* site and the O–H bond is perpendicular to the c-axis (figure 4) [24]. Electron paramagnetic resonance (EPR) studies showed that the proton is located at (0.53, 0.11, 0.0) in fractional coordinates, while the O^{2-} ion to which it is bonded is located at (0.8053, 0.3053, 0.0). The O–H bond length was determined to be 0.109 nm [49]. These results agree well with theoretical calculations [24].

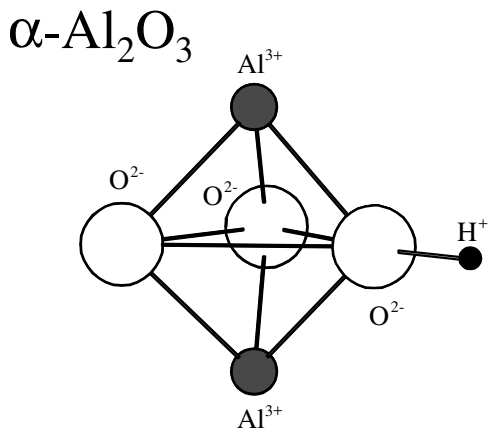

Figure 2. Schematic drawing of the aluminium oxide molecular unit showing the H^+ interstitial site. (After [26].)

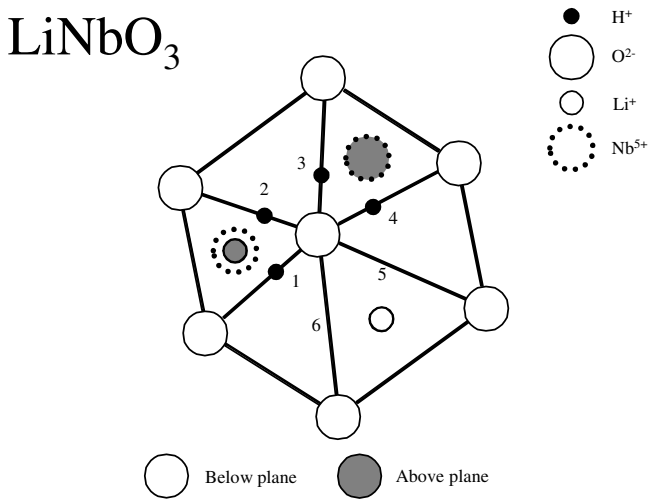

Figure 3. Schematic depiction of the oxygen plane perpendicular to the ferroelectric *c*-axis in $LiNbO_3$ crystals. The proton locations are indicated. (After [47].)

3. Experimental details

Diffusion studies of hydrogen isotopes were performed in crystals of MgO, Al_2O_3, $LiNbO_3$ and TiO_2. Infrared absorption (or transmission) was used to monitor the presence of hydrogen and its isotopes which are present in the form of OH^-, OD^- and OT^- radicals. Assuming a harmonic oscillator model for the stretching vibrations of these radicals, the ratio of the stretching frequencies is $[\mu(OD^-)/\mu(OH^-)]^{1/2} = 1.37$ and $[\mu(OT^-)/\mu(OH^-)]^{1/2} = 1.64$. Here μ is the reduced mass of the radicals. In MgO, $[H^-]^+$ centres also absorb in the infrared. Supporting roles were played by other techniques such as optical absorption in the UV–Vis, which provides information on the electronic transitions, and EPR, which detects point defects with unpaired spins.

In most experiments, deuterons originating from a D_2O atmosphere were used as tracers in order to distinguish them from either protons inherently present in the crystals or the electrical

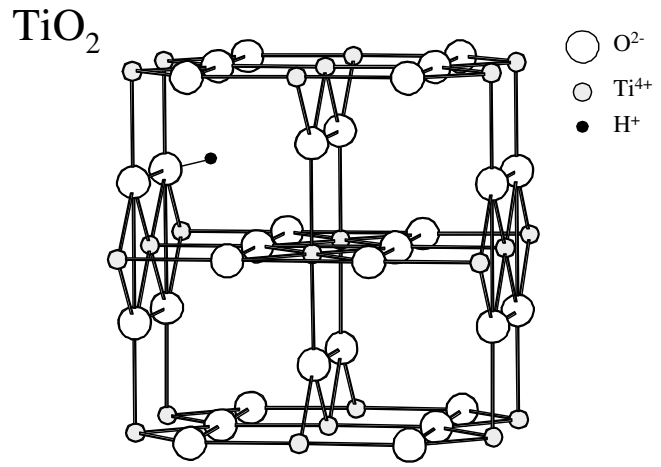

Figure 4. Rutile lattice showing the position of the proton. (After [24].)

contacts. Tritium ions have been produced in $LiNbO_3$ crystals by transmutation of ^{6}Li ions by thermal neutrons according to the following nuclear reaction

$$^6_3\mathrm{Li} + {}^1_0n \rightarrow {}^3_1T + {}^4_2\mathrm{He} \tag{1}$$

with a production cross-section of 910 barns [50]. The natural abundance of the $^6_3$Li isotope is 7.4%.

The electron irradiation source was a 2.0 MeV van de Graaff electron generator. Room-temperature irradiations were carried out in a sample holder using tap water as a coolant, and the low-temperature irradiations were performed in a cryostat cooled by liquid nitrogen. The temperature of the sample during irradiation was estimated to be about 290 and 85 K respectively.

4. Mathematical formalism

The diffusion characteristics for a classical system with a low concentration of defects or impurities such that they do not interact with each other can be described by Fick's second law. In one dimension it can be written as [51]

$$\frac{\partial C}{\partial t} = D\frac{\partial^2 C}{\partial^2 x} \tag{2}$$

where C is the concentration of the diffusing species, x is the coordinate and D is the diffusion coefficient. For dilute systems, D can be considered independent of C. At time t the total concentration of the diffusing species in a sample of thickness $2\,d$ and area S ($d \ll S$) is given by

$$C(t) = \frac{1}{2d}\int_{-d}^{d} C(x,t)\,\mathrm{d}x \tag{3}$$

where $C(x,t)$ is the concentration of the diffusing species at annealing time t. $C(t)$ is proportional to the experimental optical absorbance, $A(t)$, of the OH^-, OD^- and OT^- bands in the sample. Here we are dealing with the *out*- and *in*-diffusion of hydrogen isotopes.

(a) In-diffusion. Under our experimental conditions, $Dt \ll d^2$, the solution of equations (2) and (3) can be approximated to be [51]

$$\frac{C(t) - C_0}{C_s - C_0} = \frac{2}{d\sqrt{\pi}}\sqrt{Dt} \tag{4}$$

where C_o and C_s are the concentrations of the diffusing species at $t = 0$ and at saturation respectively. Hence the in-diffusion coefficient can be obtained from the formula

$$D_{in} = \left(\frac{d}{2}\right)^2 \frac{\pi m^2}{(A_\infty - A_0)^2} \tag{5}$$

where m is the initial slope for a plot of absorbance versus $t^{1/2}$ and A_0 and A_∞ are the absorbance at $t = 0$ and at saturation.

(b) Out-diffusion. The diffusion equation is as follows [51]:

$$C(x,t) = \frac{4C_0}{\pi}\sum_{n=0}^{\infty}\frac{(-1)^n}{2n+1}\exp\left(-\frac{D_{out}(2n+1)^2\pi^2 t}{4d^2}\right)\cos\left(\frac{2n+1}{2d}\pi x\right). \tag{6}$$

Integration of equation (3) yields

$$C(t) = \frac{8C_0}{\pi}\sum_{n=0}^{\infty}\frac{1}{(2n+1)^2}\exp\left(-\frac{D_{out}(2n+1)^2\pi^2 t}{4d^2}\right). \tag{7}$$

Retaining the first term of equation (7), the out-diffusion coefficients can be calculated from the slope M of a semilog plot of $A(t)$ against isothermal annealing time using the expression

$$D_{out} = \frac{4Md^2}{\pi^2}. \tag{8}$$

This approximation is satisfied within an error of 10% under the condition $Dt > 0.005d^2$.

5. MgO single crystals

In recent decades the properties of MgO crystals have been extensively studied with a multitude of experimental techniques because of their simple sodium chloride crystalline structure and technological applications. These applications include support for metal catalysts, thin film formation, high temperature superconductors and as an insulator in different parts of advanced fusion devices. In particular, considerable effort has been devoted to studying the transport of hydrogen isotopes in MgO single crystals.

5.1. Thermal diffusion

Internal redistribution, in-diffusion and out-diffusion of hydrogen isotopes were investigated in MgO crystals. Hydroxyl configurations are observed to be stable at room temperature and protons do not diffuse until 800 K [17, 38]. MgO crystals with a large hydrogen content were produced by presoaking the starting MgO powder with water [52]. The resulting crystals are very cloudy due to the presence of cavities containing high-pressure hydrogen gas [41, 42]. As indicated previously, the two most prominent IR absorption bands in as-grown MgO:H peak at 3296 and 3700 cm^{-1} (figure 5), and have been associated with V_{OH}^- centres and $Mg(OH)_2$ precipitates respectively. The full width at half maximum (FWHM) of these two bands is 7 and 12 cm^{-1} respectively. At high temperatures, protons are randomly distributed throughout the crystal and freeze in their substitutional sites during fast cooling, thus forming V_{OH}^- centres. However, if the crystal is cooled slowly the protons will move around and have ample opportunity to aggregate in $Mg(OH)_2$ precipitates [17].

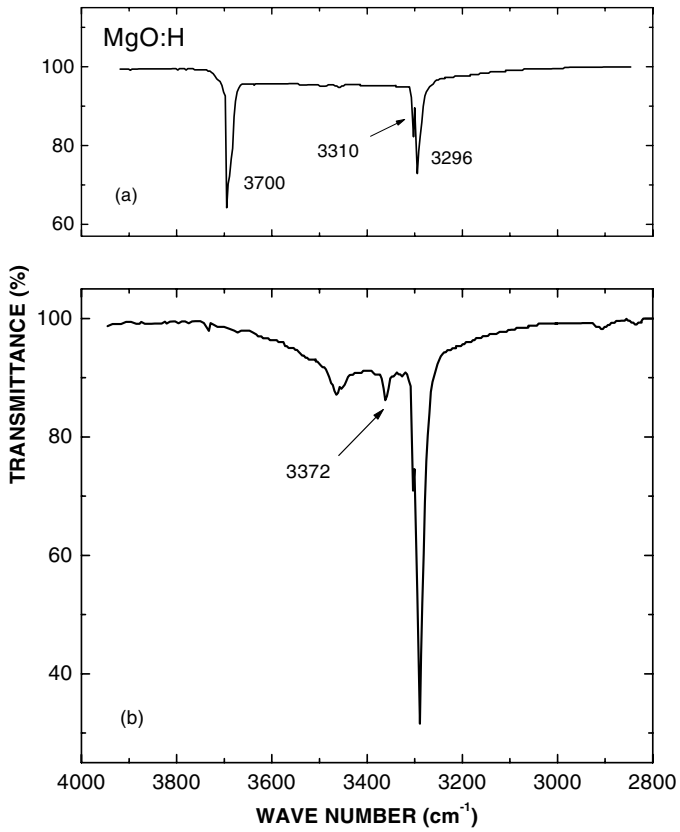

Figure 5. Infrared spectra of MgO crystals containing hydrogen after (a) slow cooling from 1400 K and (b) fast cooling from 1450 K. (After [17].)

Figures 5 and 6 illustrate the internal redistribution of protons at elevated temperatures. Figure 5(a) shows the IR transmission spectrum of an MgO:H crystal after it was cooled slowly from 1400 K to room temperature over a 24 h period. After heating to 1450 K and quenching into a bath of liquid nitrogen the crystal exhibits the spectrum shown in figure 5(b). The relative intensities of the 3296 and 3700 cm^{-1} bands are reversible indefinitely by alternate slow cooling and quenching. As expected, slow cooling resulted in an increased absorption for the 3700 cm^{-1} band an a decrease in the 3296 cm^{-1} signal. The converse is true for quenching.

Figure 6 illustrates the thermal behaviour of the 3296 cm^{-1} band at intermediate annealing temperatures. The lower curve (a) represents the absorption coefficient of the band when the sample was initially cooled slowly and subjected to isochronal annealing for 10 min at each increasing temperature. After each anneal, the crystal was quenched into liquid nitrogen. Up to $\approx$800 K the absorption coefficient remained unchanged. At higher temperatures, the protons were sufficiently energetic that they could diffuse and occupy substitutional sites, thereby enhancing the intensity of the 3296 cm^{-1} band. At $T > 1200$ K a saturation effect emerges. On the other hand, when the crystal was initially quenched from 1450 K and isochronally annealed in the same manner, the absorption coefficient varied as shown in (b). Again at $T < 800$ K no change in absorption was noted, indicating a lack of mobility of the substitutional protons. At 800 K substitutional protons escape and find other preferred sites such as $Mg(OH)_2$. An inversion of the curve occurred at 900 K. At higher temperatures, the protons become energetic

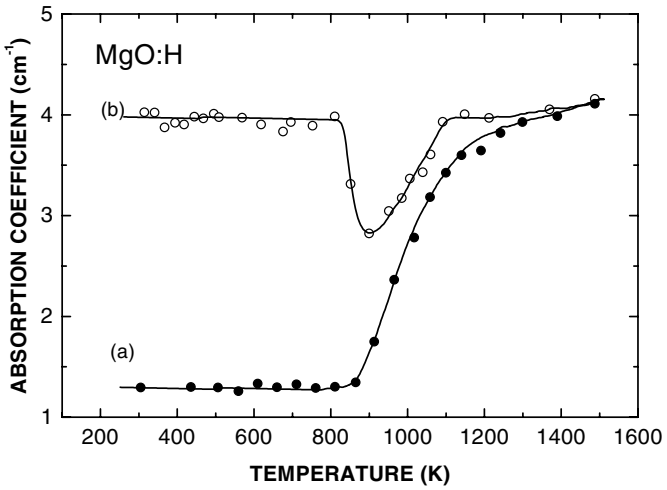

Figure 6. Absorption coefficient of the 3296 cm^{-1} band as a function of isochronal annealing temperature for a hydrogen-containing MgO crystal (a) initially slow cooled and (b) fast cooled from 1450 K. (After [17].)

enough to occupy more and more substitutional sites. The curves in figure 6 indicate that at $T <$ 800 K protons are not sufficiently energetic to incur a redistribution of substitutional protons.

We shall next analyse the *in*- and *out*-diffusion of hydrogen isotopes in MgO crystals. The minimum temperature at which deuterons diffuse into MgO crystals, doped or undoped, was observed to be ≈1750 K, with heating times of 1 h. The exception is MgO:Li for which the minimum temperature is ≈800 K. It is also noted that for MgO:H (cloudy crystals) which had high OH^- concentrations, the amount of deuterium that diffused into the crystal was higher than in crystals with low OH^- concentrations. For these reasons the emphasis in the diffusion studies was placed on undoped MgO, MgO:H and MgO:Li. The results for the anomalous MgO:Li crystals will be presented in section 5.1.2.

The spectra of nominally pure MgO and hydrogen-doped MgO crystals after being annealed in D_2O vapour are shown in figure 7. In the undoped MgO crystal, the V_{OH}^- signal at 3296 cm^{-1} was completely removed and the deuterium analogue of this band at 2445 cm^{-1} emerged. In the MgO:H crystal the intensities of the OD^- bands were considerably greater. The ratio of the frequencies for a given defect is 1.35 which corresponds well with the theoretical expectation of 1.37 for the two isotopes. The slight departure from 1.37 is indicative of the anharmonicity of the oscillators.

Figure 8 plots the OD^- absorbance $A(t)$, monitored by the 2445 cm^{-1} band, versus $t^{1/2}$ for an undoped MgO and a MgO:H crystal following annealing in D_2O vapour at 1873 K. The linearity of the two plots indicates the validity of the $t^{1/2}$ dependence. The diffusion coefficients, D, were calculated from the slopes m and the absorbance at saturation using equation (5). The values obtained are $D(\mathrm{MgO}) = (1.4 \pm 0.5) \times 10^{-6}$ cm^2 s^{-1}, and $D(\mathrm{MgO:H}) = (0.9 \pm 0.4) \times 10^{-6}$ cm^2 s^{-1}. For values of the diffusion coefficient equal to or less than 10^{-6} cm^2 s^{-1} and thicknesses of about 0.1 cm, the condition imposed in section 4, $Dt \ll d^2$, is satisfied. We conclude there is no substantial difference in the diffusion coefficients between these two crystals.

5.1.1. Isotopic effect. Classically, the diffusion coefficient of protons is expected to be larger than that of deuterons because of the smaller mass. However, this is not necessarily true since

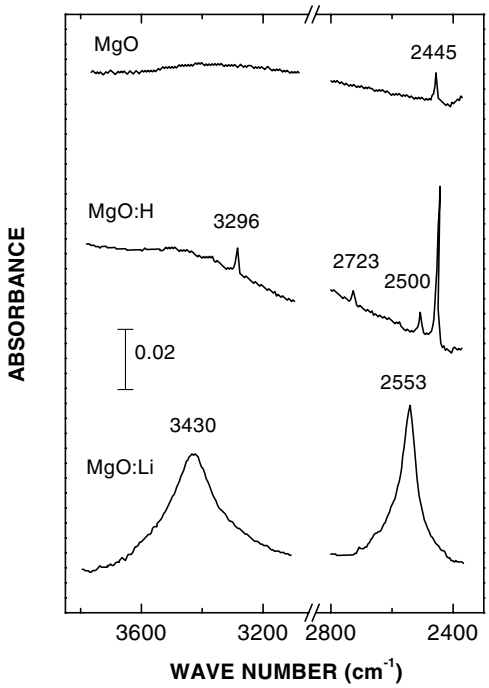

Figure 7. Absorption spectra of an undoped MgO crystal (top) and an MgO:H crystal (centre), after both had been heated in D_2O vapour at 1830 K for 30 min. The spectrum at the bottom corresponds to an MgO:Li crystal after deuteration at 1173 K for 30 min. (After [28].)

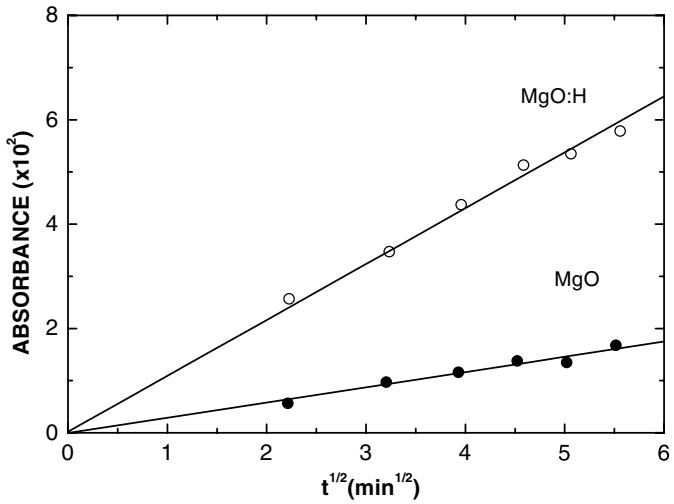

Figure 8. Absorbance of OD^- ions at 2445 cm^{-1} against $t^{1/2}$ for MgO and MgO:H crystals following anneals at 1873 K. Thicknesses of the crystals were 0.152 and 0.156 cm respectively. (After [28].)

there are systems where the opposite has been observed: for example fcc metals in certain temperature ranges [53]. The reasons for this were attributed to quantum effects [54, 55].

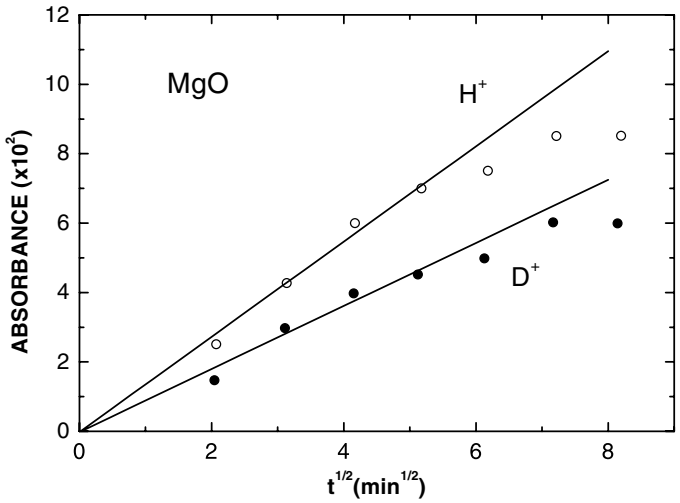

Figure 9. Absorbance of the 3296 and 2445 cm^{-1} bands against $t^{1/2}$ for a hydrogen-free MgO crystal heated in a mixture of D_2O and H_2O vapour at 1873 K. The sample thickness was 0.146 cm. (After [28].)

To establish experimentally the ratio $D(H^+)/D(D^+)$, experimental conditions which are *exactly identical* for both hydrogen and deuterium diffusion were chosen. An undoped clear crystal was initially heated at 1873 K in flowing oxygen for several hours until all traces of OH^- bands disappeared. The crystal was then isothermally annealed at 1873 K in an atmosphere comprising comparable concentrations of D_2O and H_2O. The absorbances at 3296 and 2445 cm^{-1} were measured after each anneal and plotted against $t^{1/2}$ in figure 9. While the slope of the OH^- curve is higher than that of the OD^-, the saturation value is also higher. The $D(H)/D(D^+)$ is determined to be 1.1 ± 0.1. Experimental factors which affect the OD^- absorbance affect the OH^- absorbance in exactly the same manner. The departure from a straight line for each anneal is comparable. Hence, there is little uncertainty in determining the ratio. It is conclude that there is no appreciable difference between $D(D^+)$ and $D(H^+)$ at 1873 K.

5.1.2. Impurity effects. Anomalous MgO:Li. Lithium-doped MgO crystals have a strong affinity for hydrogen. Apart from the unsuccessful efforts to remove hydrogen completely from these crystals during crystal growth, IR absorption measurements (figure 7) have shown a broad absorption band (the FWHM is 185 cm^{-1}) centred at 3430 cm^{-1}, which is probably due to O–H configurations perturbed by distant lithium ions [28, 56]. The sharp lines at 3296 and 3700 cm^{-1}, which represent the most common frequencies observed in lithium-free hydrogen-containing crystals, were not detected. After deuteration, a broad band peaking at 2553 cm^{-1} is observed (figure 7). The ratio of the frequencies of the two broad bands is 1.34.

The lowest temperature for deuterium to diffuse into MgO:Li under our experimental conditions is ≈800 K, as shown in figure 10. A crystal was isochronally annealed for 5 min intervals at increasing temperatures in D_2O vapour. After each anneal, the OD^- and the OH^- concentrations were monitored by their respective bands. Figure 10 shows that the OD^- concentrations increased at the expense of the OH^- concentrations. In fact, the two curves give an appearance of a mirror reflection of one another, suggesting that the mechanism is a replacement or exchange process. Also, the temperature at which OH^- concentration begins to diminish corresponds well to the lowest temperature for deuterium diffusion.

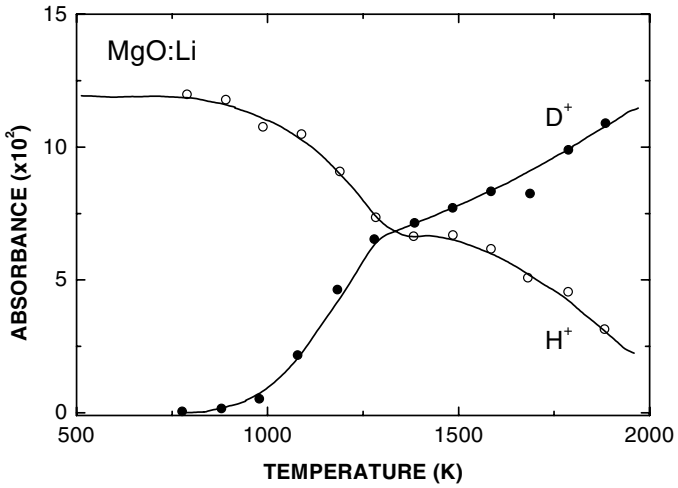

Figure 10. Absorbance of OD^- and OH^- ions versus isochronal annealing temperature for an MgO:Li crystal. (After [28].)

Isothermal annealing in D_2O vapour was performed in three MgO:Li crystals at 1073, 1123 and 1173 K respectively. After each annealing, the concentration of deuterium was measured. Using the cross-cut method [57] an activation energy $E = 1.9 \pm 0.2$ eV was obtained. Plotting the absorbance versus $t^{1/2}$ for the 1173 K annealing, the diffusion coefficient was found to be $D = (1.0 \pm 0.4) \times 10^{-6}$ cm^2 s^{-1}. These results provide strong evidence that protons (deuterons) are more mobile in the presence of lithium impurities in MgO. The reason for this has not been clearly addressed.

5.2. Sweeping by electric field

Removal of hydrogen from oxides is much more effective by application of an electric field, especially for materials with open channels such as quartz [58]. Here, we will show that H^+ or D^+ can also be removed effectively from a tight lattice such as MgO. Five transparent samples of the same thickness containing moderate numbers of OH^- ions were used. Each was heated at a different temperature for 70 min in a dry nitrogen atmosphere. During the heat treatment, a field of 2000 V cm^{-1} was applied to part of the crystal so that the area without an electric field could be used as a control. The results are shown in figure 11. Out-diffusion of hydrogen is apparent at $T = 1100$ K or higher. Removal of hydrogen is much more effective with an applied field.

A study of the hydrogen profiles on the field-induced areas of the samples showed that most of the hydrogen concentrated near the negative electrode. This observation is consistent with the expectation that protons are swept toward the region of negative polarity.

5.3. Radiation induced diffusion

We have already demonstrated that OH^- ion configurations are stable up to 800 K. However, we will shown in this section that OH^- ions become highly unstable during ionizing radiation at room temperature resulting in the displacement of protons [17, 39, 59].

The effect of electron irradiation at $T \approx 290$ K for several selected doses is illustrated in figure 12. An MgO:H crystal was initially quenched from 1450 K to maximize the intensity of the absorption band at 3296 cm^{-1}, as shown in the spectrum in figure 5(b). Subsequently,

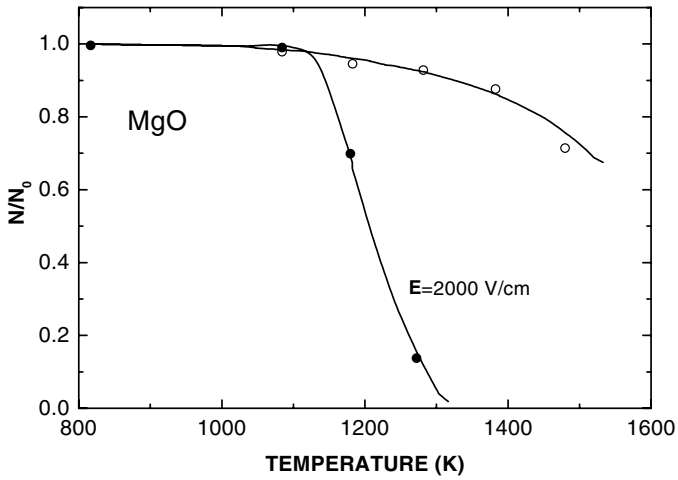

Figure 11. Normalized concentrations of OH^- ions in MgO versus annealing temperature with and without an applied electric field. (After [28].)

it was irradiated with electrons in small doses until it reached 2.6×10^{18} e cm^{-2}. During irradiation the intensity of the 3296 cm^{-1} band decreased, with most of the decrease occurring during the initial dose of 1×10^{16} e cm^{-2}. The decay of this band was accompanied primarily by an increase in the 3697 cm^{-1} band (commonly referred to as 3700 cm^{-1}). The electron irradiation causes the proton to relocate from its substitutional site to the $Mg(OH)_2$ precipitate site. The variation of the 3296 cm^{-1} band intensity at 290 K as a function of the electron dose is plotted at the bottom of figure 13. A similar experiment was performed at $T \approx 85$ K, but measured at room temperature. The decay of the 3296 cm^{-1} band is plotted at the top of figure 13. It is evident that the decrease in absorption at the higher temperature is much more rapid.

The displacement cross-section σ of the substitutional protons can be determined [39] by use of the relationship $\sigma = (\Delta C/C)/\Delta\phi$, where C is the initial concentration of the substitutional protons in the crystal and $\Delta C/\Delta\phi$ is the number of displacement events per cubic centimetre for a given irradiation dose. Since $\Delta C/C$ is equal to the fractional loss of the 3296 cm^{-1} absorption band, the cross-sections can be determined from the initial slopes of the two decay curves. From the slope of the 290 K irradiation shown in figure 13 (not fully expanded in order that the decay curves for the two temperatures can be compared on a common abscissa), a cross section of $\geqslant 3 \times 10^8$ barns (1 barn $= 10^{-24}$ cm^2) was obtained. For the 85 K irradiation, a value of $\approx 10^6$ barns was determined.

To compare the displacement probabilities of protons and deuterons, an MgO crystal containing both isotopes was initially quenched from 1450 K to maximize the V_{OH}^- and V_{OD}^- concentrations. It was subsequently irradiated with electrons at 290 K. The advantage of using one crystal is that the experimental conditions, such as irradiating temperature, beam intensity and dose, are identical for both hydrogen and deuterium. For all intents and purposes the essential difference lies in the mass and the resulting mobility. Measurements were also made after electron irradiation at different doses. The displacement cross-section of hydrogen at 290 K was determined to be twice that of deuterium [39]. Hence we conclude that the proton because of its lower mass, is displaced more readily than the deuteron. Whereas the isotopic effect is minimal for thermal diffusion as previously noted, for RID it is substantial.

Ionizing irradiation has the effect of breaking the O–H bond with phenomenal efficiency. The enormous cross-section for the RID appears to have no precedent. The mechanism by

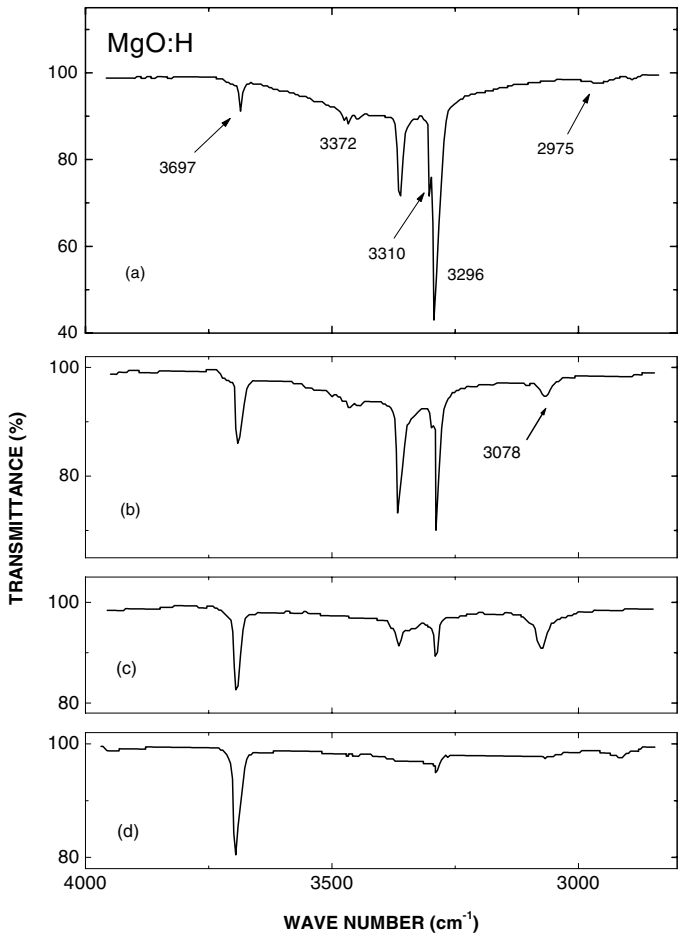

Figure 12. Infrared spectra of fast-cooled MgO:H crystal at $T = 290$ K after electron irradiation to doses of (a) 3.1×10^{15}, (b) 2.9×10^{16}, (c) 4.4×10^{17} and (d) 2.6×10^{18} e cm^{-2}. (After [17].)

which the protons or deuterons are displaced from their sites unmistakably involves ionization (sometimes also referred to as photochemical ionization or radiolysis) rather than elastic collisions. First, the cross-section of 10^8 barns, and for that matter also 10^6 barns at 85 K, is far too large to be associated with elastic collisions. The theoretical cross-sections for displacements by elastic collisions are of the order of a few barns for $\approx$2.0 MeV electrons, and experimental cross-sections are almost always much lower, because of annihilation by interstitial–vacancy recombination. Secondly, subthreshold-energy x-rays (20 kV peak) were also found to be capable of displacing the protons from their sites. Thirdly, irradiation with both low- and high-energy photons showed that there was no energy dependence in the decay of the 3296 cm^{-1} band. A cross-section of 10^8 barns requires a displacement mechanism involving capture of secondary electrons or holes created by the incident electrons. (On the average, an electron–hole pair per 100 nm is created by each irradiating electron.) The strong temperature dependence of proton displacement is indicative of a thermally activated process of escape, probably involving a neutral hydrogen atom rather than a proton which would have to overcome a large Coulombic barrier. The availability of an abundance of electrons and holes

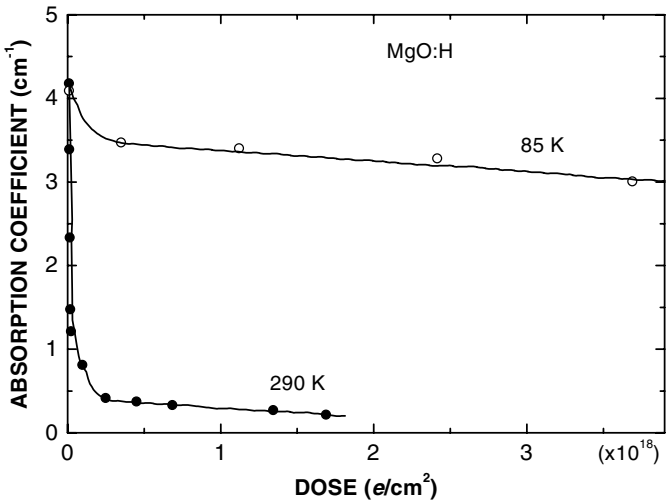

Figure 13. Decay of the 3296 cm^{-1} absorption band in a MgO:H crystal as a function of electron dose for two irradiating temperatures. (After [39].)

makes it easy for the protons to frequently change their valence and thus avail themselves of the opportunity to become hydrogen atoms. The subsequent migration to aggregate at precipitates is more likely in the form of protons ($r \approx 10^{-13}$ cm) than monatomic H ($r \approx 10^{-8}$ cm).

5.4. Hydride ions

5.4.1. Defect production and stability. The preceding discussions address protons forming *hydroxyl* ions in MgO crystals. We shall now discuss protons occupying substitutional *anion* vacancies in MgO, also referred to as hydride ions. Thermochemical reduction (TCR) at high temperatures (>2000 K) and high pressure (≈7 atm of Mg vapour) in a tantalum vessel leads to a stoichiometric deficiency of oxygen ions, resulting in oxygen vacancies. Some of the hydrogen in the crystals is trapped at these vacancies, forming $[H^-]^+$ centres. The presence of these centres greatly modifies the optical properties of the crystals [60].

$[H^-]^+$ centres are identified by sharp absorption lines in the low-energy infrared spectrum which can be attributed to the fundamental vibrations of substitutional H^- ions. At 295 K the peaks occur at 1053, 1032, and 1024 cm^{-1} (figure 14(a)) [43]. The presence of three sharp, closely spaced bands (none intensity correlated) indicates that they are of different species presumably with different impurity compensators [40]. Hereafter, we will distinguish between the substitutional $[H^-]^+$*centre* (a proton with two electrons in an O^{2-} vacancy) and the interstitial H^-*ion* (a proton with two electrons in an interstitial position).

The thermal stability of $[H^-]^+$ centres was determined by subjecting two thermochemically reduced crystals to isochronal anneals of 10 min duration in either reducing or oxidizing atmospheres (figure 15). The initial $[H^-]^+$ concentration of these crystals was estimated to be $\approx 2.9 \times 10^{18}$ cm^{-3} [40]. In oxygen, all the $[H^-]^+$ vanished by 1800 K [61, 62]. In a reducing atmosphere, the concentration remained unchanged even at 1923 K [40].

5.4.2. Thermal diffusion. In order to determine the activation energy for the diffusion of $[H^-]^+$ centres, isothermal annealing of 5 min duration in flowing oxygen at 1530, 1630 and 1750 K was performed on three crystals with the same thickness and the same initial $[H^-]^+$

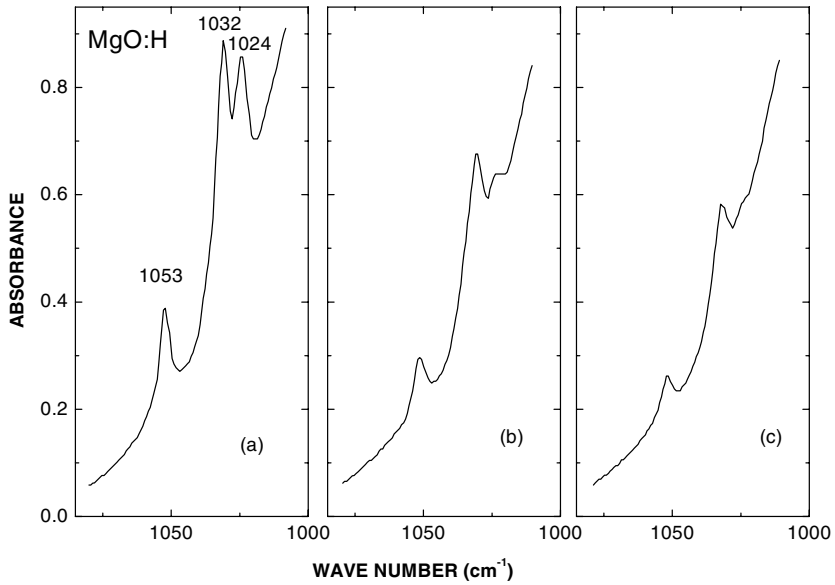

Figure 14. Infrared spectra for $[H^-]^+$ centres in MgO:H (a) prior to electron irradiation, and after electron irradiations with cumulative doses of (b) 5×10^{16} cm^{-2} and (c) 2×10^{17} cm^{-2}. (After [40].)

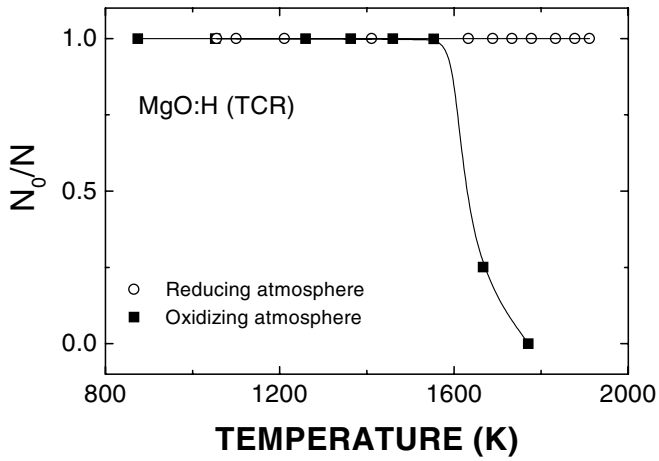

Figure 15. Normalized concentration versus isochronal annealing temperature of two thermochemically reduced MgO:H samples in a reducing atmosphere and in flowing oxygen. (After [61].)

concentration. The activation energy for the annealing-out of $[H^-]^+$ centres was obtained using the cross-cut method [57]. For the three bands it was found to be $E(1024\,\mathrm{cm}^{-1}) = (1.4 \pm 0.2)$, $E(1032\,\mathrm{cm}^{-1}) = (1.5 \pm 0.3)$ and $E(1053\,\mathrm{cm}^{-1}) = (1.4 \pm 0.2)$ eV respectively. The decay curves of the $[H^-]^+$ centres are poorly fitted to a single exponential, which indicates that the annealing of the $[H^-]^+$ centres does not occur by a first-order reaction.

In the simulations of the $[H^-]^+$ centres [62, 63], the embedded molecular cluster model was used in conjunction with an *ab initio* molecular orbital theory based on the Hartree–Fock (HF) formalism. This method is similar to the DICAP code which was found to be very useful

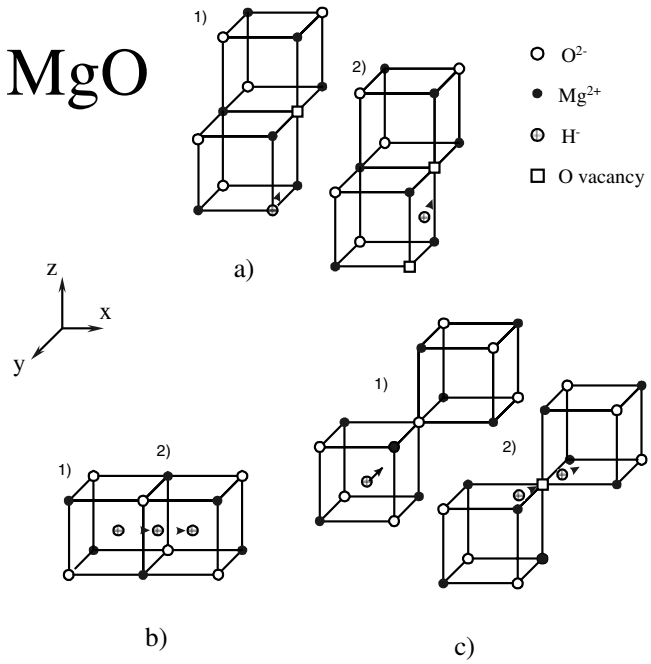

Figure 16. (a) Vacancy mechanism of the substitutional $[H^-]^+$ centre diffusion: (1) the initial (ground state), (2) the saddle point. (b) Direct jump of the H^- interstitial through the cube face during the [100] hop. (c) Collinear interstitialcy mechanism of the H^- ion diffusion: (1) the initial state, (2) the saddle point. (After [63].)

in studies of defects in alkali halides [64]. This approach and its application to defects in MgO is described in detail in [65–68].

Calculations in conjunction with experimental results showed that the mobile defect is more compatible with the H^- ion than with the proton. Two possible mechanisms were modelled (figure 16) [63]. First, a *standard vacancy* mechanism (the $[H^-]^+$ centre exchanges with an O^{2-} vacancy) was found not to be energetically feasible since that position exchange requires a very large activation energy. Second, a *direct interstitialcy* mechanism requires that the H^- ion leaves its oxygen vacancy, becomes an interstitial and subsequently hops along the [100] axis. This mechanism yields an activation energy of $\approx$3 eV, twice that measured experimentally. The authors suggest that a *collinear interstitialcy* mechanism (the interstitial hydride ion hops along the [111] axis and in its saddle point forms a dumbbell with an O^{2-} ion in a regular site) could provide an activation energy closer to the experimental value. However, for an asymmetric H^-–O^{2-} dumbbell, it is not easy to optimize the defect geometry at the saddle point. Alternatively, the motion of the H^-–oxygen vacancy complex is also considered. This correlated motion can be characterized by the activation energy which is probably smaller than those for the individual defects.

5.4.3. Radiation induced diffusion. Ionizing radiation displaces protons from $[H^-]^+$ centres with a cross-section comparable to that from substitutional cation sites [40]. Electron irradiations were performed on a thermochemically reduced MgO:H crystal after it had been heated at 1900 K in a reducing atmosphere to anneal out the oxygen vacancies. Therefore the crystal contained a large concentration of $[H^-]^+$ centres but no anion vacancies. Three irradiations

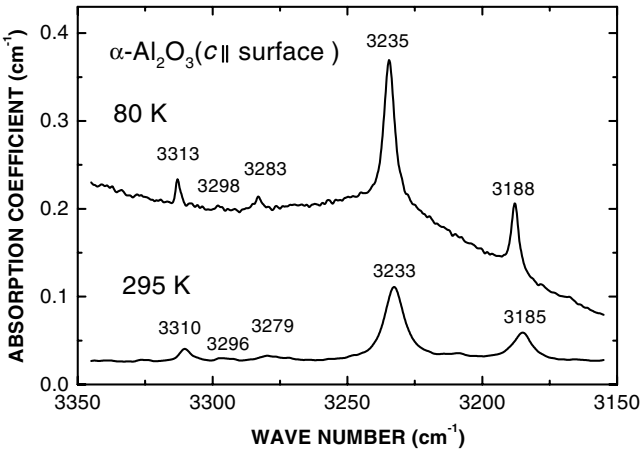

Figure 17. Absorption spectra of an as-grown α-Al_2O_3 crystal ($c \parallel$ surface) measured at room temperature (bottom) and at 80 K (top). (After [37].)

were carried out, corresponding to cumulative doses of 4×10^{15}, 5×10^{16} and 2×10^{17} e cm^{-2}. The infrared spectra before and after two of the irradiations are shown in figure 14. The net effects of the irradiation are: (1) creation of new anion vacancies, (2) a decrease in the absorbance in the $[H^-]^+$ spectra and (3) appearance of new OH^- bands. These effects are aspects of the same RID process which involves the displacement of protons in the $[H^-]^+$ configurations and their relocation elsewhere in the crystal as OH^+ ions. Assuming that the displacement of one proton from an $[H^-]^+$ centre results in the formation of one anion vacancy, a cross-section of $\approx 1 \times 10^{18}$ barn is determined, corresponding to a factor of 10^9 greater than that for the elastic collision displacement of oxygen [69]. A cross-section of this magnitude is uniquely characteristic of RID of protons (or deuterons) [39], albeit in this case from anion sublattice sites.

6. α-Al_2O_3 single crystals

Due to its strength and high melting temperature, Al_2O_3 is a particularly suitable candidate for first-wall material in fusion devices and for hydrogen-containment purposes. The infrared absorption spectra of a virgin α-Al_2O_3 crystal are shown in figure 17. In order to observe fine structures, a thick crystal (23 mm) was used [37]. The spectrum at 295 K is shown at the bottom. A prominent band at 3233 cm^{-1} with a FWHM of $\approx$9 cm^{-1} is observed. Four satellite bands at 3185, 3279, 3296 and 3310 cm^{-1} are also apparent. The spectrum at 80 K is shown at the top. The notable features are: the band peaks shifted toward higher energies, intensities enhanced and bands narrowed.

6.1. Thermal diffusion

Figure 18 illustrates the absorption spectra in the OD^- regime at two temperatures [37]. Again these bands are better resolved at 80 K. The ratio of the frequencies is $\approx$1.34. The slight departure from 1.37 is indicative of the anharmonicity of the oscillators. Polarization experiments show that the OH^- and OD^- ions lie in the basal plane in agreement with [26]. The different OH^- bands and their OD^- analogues are probably due to perturbations by nearby impurities.

For the diffusion experiments in a D_2O atmosphere the samples had a thickness of about 1.3 mm. In these relatively thin samples, of all the five OH^- (OD^-) bands only the OH^-

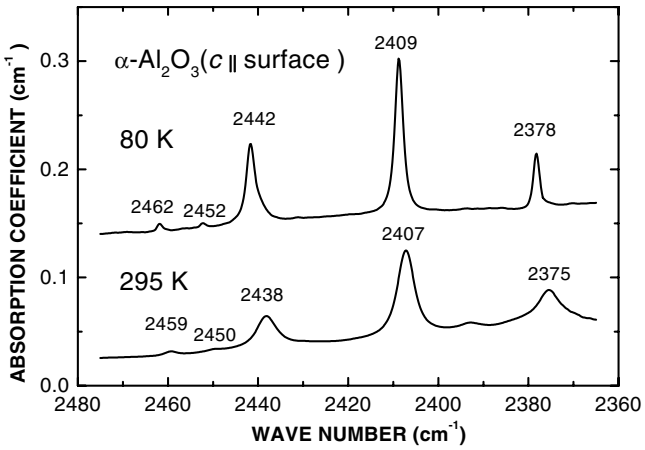

Figure 18. Absorption spectra of the α-Al_2O_3 crystal of figure 17, after deuteration, measured at room temperature (bottom) and at 80 K (top). The deuteration was performed at 1373 K for 15 h at $\approx$800 V cm^{-1} along the c direction. (After [37].)

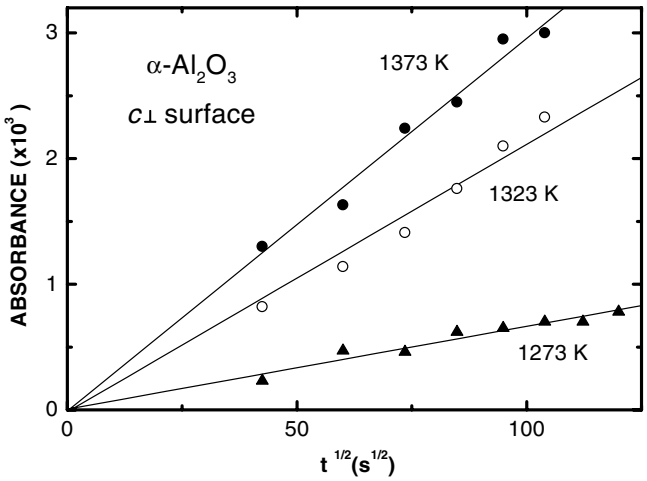

Figure 19. Absorbance of OD^- ions versus $t^{1/2}$ at three temperatures for α-Al_2O_3 crystals ($c\perp$ surface) annealed in D_2O vapour at 1273, 1323 and 1373 K. The crystals have a thickness of 0.13 cm. (After [37].)

band at 3233 cm^{-1} and its OD^- analogue at 2407 cm^{-1} were observed. The absorbance of the 2407 cm^{-1} band is plotted against $t^{1/2}$ for three sapphire crystals ($c\perp$ surface), each of which was isothermally annealed at 1273, 1323 and 1373 K (figure 19). From the slopes, the diffusion coefficients in the c direction were determined to be $D(1273\,\mathrm{K}) = 1\times10^{-8}$ cm^2 s^{-1}, $D(1323\,\mathrm{K}) = 8\times10^{-8}$ cm^2 s^{-1} and $D(1373\,\mathrm{K}) = 20\times10^{-8}$ cm^2 s^{-1}. The activation energy E for the deuterium diffusion was obtained using the cross-cut method [57], and the resulting value was $\approx$5 eV. An activation energy of 5 eV suggests that the deuteron (proton) diffusion is associated with the motion of Al^{3+} vacancies which has also been observed to occur with an activation energy of 5 eV [70–72].

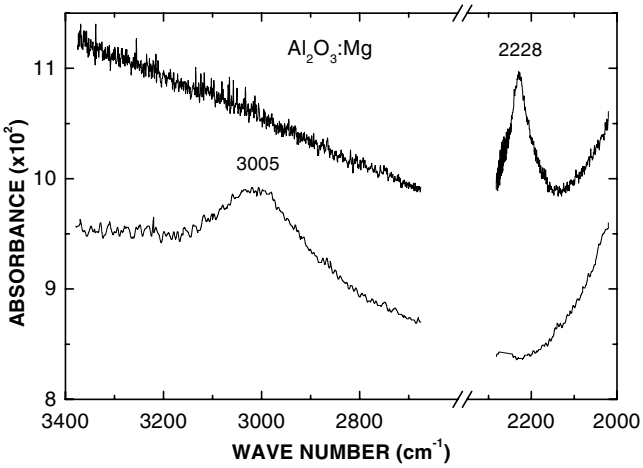

Figure 20. Infrared absorption spectra of an Al_2O_3:Mg crystal (random oriented) before (lower portion) and after (upper portion) exposure to flowing D_2O vapour for 60 min at 1273 K. (After [38].)

6.1.1. Crystal orientation dependence. Experiments with crystals with an orthogonal crystallographic orientation ($c \parallel$ surface) were also performed. We conclude that deuteron in-diffusion perpendicular to the c-axis was at least 50 times smaller than the in-diffusion parallel to the c-axis.

6.2. Magnesium-doped Al_2O_3 crystals

Al_2O_3:Mg crystals exhibit some similarities to MgO:Li crystals. In particular, $[Mg]^0$ centres [73, 74] (a substitutional Mg ion with a trapped hole localized at one of the six neighbouring O^{2-} ions) in Al_2O_3:Mg behave like $[Li]^0$ centres [75–77] (a substitutional Li^+ ion with a hole trapped at an adjacent O^{2-} ion) in MgO. These trapped-hole centres are responsible for the p-type semiconducting properties observed in these oxides at temperatures above room temperature [78, 79]. It therefore is important to characterize hydrogenic species in Al_2O_3:Mg and to investigate whether the presence of substitutional Mg ions enhances the diffusion of hydrogen isotopes.

The infrared absorption of an as-grown Al_2O_3:Mg crystal before and after deuteration is shown in figure 20. This crystal has a 'random' orientation, but was characterized to have the c-axis and the normal direction to the broad sample surface forming an angle of $\approx 50°$. The concentration of Mg in the crystals is of the order of 25 appm [38]. The spectrum before deuteration is shown in the lower half of figure 20. A very broad band centred at about 3005 cm^{-1} with a FWHM of 220 cm^{-1} is observed [38]. This width is much larger than the 4–9 cm^{-1} in magnesium-free crystals. After 60 min in D_2O vapour at 1273 K, a broad band attributable to OD^- ions appears at about 2228 cm^{-1}. The OH^- band has practically disappeared (figure 20 top). The frequency ratio of the OH^- to OD^- band is 1.35.

In both MgO:Li and in Al_2O_3:Mg crystals the OH^- (OD^-) band is much broader than is observed in the corresponding undoped crystal. In MgO:Li the OH^- (OD^-) band has been attributed to Li^+-associated OH^- (OD^-) ions. By analogy, we attribute the infrared OH^- (OD^-) bands in Al_2O_3:Mg crystals to Mg^{2+}-associated OH^- (OD^-) ions. However, there is a difference between the two systems. The presence of Mg^{2+} ions shifts the OH^- (OD^-) band peaks towards a lower energy than that in undoped crystals, whereas in MgO the presence of Li^+ shifts the peaks towards higher energies [28, 32, 56]. Because of its small ionic radius, the

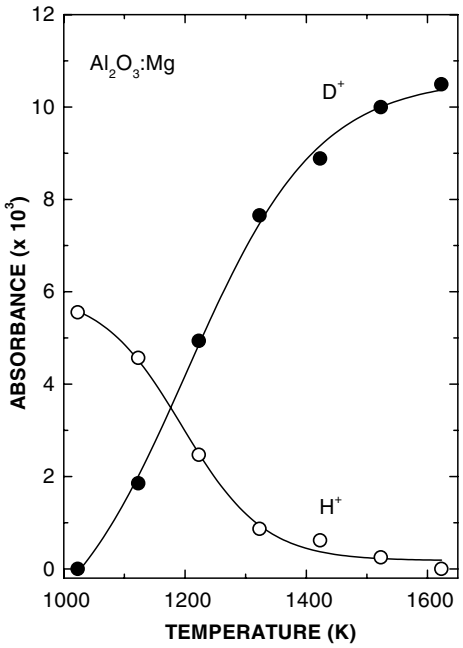

Figure 21. Absorbance of OD^- and OH^- ions versus isochronal annealing temperature for an Al_2O_3:Mg crystal. (After [38].)

presence of lithium ions in MgO produces a local inward relaxation of the lattice; in Al_2O_3:Mg, on the other hand, an outward lattice relaxation is produced because magnesium ions have a larger ionic radius than aluminium ions.

An Al_2O_3:Mg crystal was annealed in flowing D_2O vapour at increasing temperatures [38]. The OD^- band emerges at $\approx$1000 K indicating that deuterons diffuse more readily in Mg doped than in undoped crystals (figure 21). The increase in OD^- concentration correlates with a decrease in the OH^- concentration. This suggests that an exchange of D^+ for H^+ was occurring.

Activation energy and diffusion coefficients were also determined by annealing three crystals in D_2O at 1173, 1223 and 1273 K, respectively [38]. The activation energy E for the deuterium diffusion was 1.6 eV. The diffusion coefficients were determined to be $D(1173\,\mathrm{K}) = 2 \times 10^{-7}\ \mathrm{cm^2\ s^{-1}}$, $D(1223\ \mathrm{K}) = 3 \times 10^{-7}\ \mathrm{cm^2\ s^{-1}}$ and $D(1273\ \mathrm{K}) = 5 \times 10^{-7}\ \mathrm{cm^2\ s^{-1}}$. These results show that the diffusion coefficient for D^+ in Al_2O_3:Mg crystals is several orders of magnitude greater than those in undoped Al_2O_3 crystals, in accordance with previous findings [23]. The large difference in activation energies (5 eV in undoped crystals compared with 1.6 eV in Mg doped crystals) clearly indicates that a different mechanism prevails in the D^+ diffusion. In the former, deuteron (proton) diffusion may be associated with the motion of Al^{3+} vacancies [70–72]. In the latter, diffusion of hydrogenic species may be related to the motion of oxygen vacancies associated with the presence of Mg^{2+} ions, with an activation energy of $\approx$ 1.8 eV [80, 81].

6.3. Electric-field-enhanced diffusion in D_2O vapour

The in-diffusion of deuterons in α-Al_2O_3 is enhanced when a moderate electric field is applied [37]. Without an electric field, the threshold temperature for a 30 min isochronal

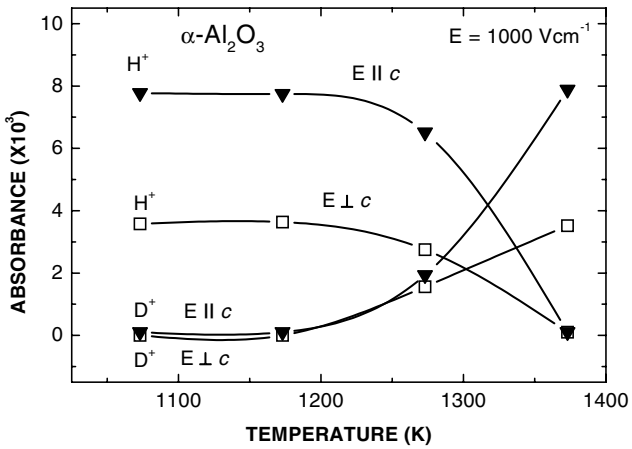

Figure 22. Absorbance of OD^- and OH^- ions versus isochronal annealing temperature for an α-Al_2O_3 crystal subjected to an electric field of $\approx$1000 V cm^{-1}. (After [37].)

diffusion was observed to be $\approx$ 1273 K. With a field of $\approx$1000 V cm^{-1}, the threshold was found to be $\approx$1200 K. Figure 22 shows that the OD^- ions increase at the expense of the OH^- ions. In fact, out-diffusion of the OH^- ions and in-diffusion of the OD^- appear to be a mirror image of one another, suggesting that the mechanism is one of replacement of protons by deuterons.

Replacement of protons by deuterons was performed as a function of electric field strength on one sample [37]. The experimental conditions were 30 min at 1300 K in D_2O with $\boldsymbol{E} \parallel c$. The effect for four electric field strengths was determined (top curve, figure 23). After each measurement, the sample was restored to its initial OH^- concentration by heating in H_2O vapour so that all D^+ ions were replaced by protons. The cycle was repeated at the next higher electric field. A linear effect was observed. Above 3500 V cm^{-1} the exchange was nearly complete. The same experiment was performed on a crystal with $\boldsymbol{E} \perp c$. Whereas purely thermal means yields in-diffusion at least 50 times lower, as noted earlier, with the addition of an applied electric field, the diffusion increased dramatically such that it was only slightly less than that for $\boldsymbol{E} \parallel c$. In the presence of an electric field there are two contributions to the D^+ in-diffusion: one due to the concentration gradient (purely thermal diffusion) and the other induced by the electric field. The former is strongly anisotropic and occurs primarily by a deuteron–proton exchange process accompanied by Al^{3+} vacancy migration. The latter diffusion becomes dominant at applied fields greater than $\approx$200 V cm^{-1} such that the effective anisotropy becomes smaller.

The present study suggests that in-diffusion of D^+ or H^+ by purely thermal means proceeds primarily via a replacement process. However, an electric field can induce in-diffusion in a crystal in which OH^- ions are undetectable. Heat treatment in D_2O vapour at temperatures as high as 1800 K did not produce OD^- ions. However, application of $E = 1200$ V cm^{-1} at 1373 K produced the 2407 cm^{-1} band [37]. This observation indicates that under the influence of an electric field deuterons can be incorporated without an exchange mechanism. Charge neutrality requires that the introduction of the positively charged deuterons (or protons) be attended by electrons trapped at impurity sites and/or defects. Luminescence experiments showed that the intensity of the Ti^{3+} emission is much weaker after deuterons were in-diffused in the crystal by application of an electric field of 1200 V cm^{-1} at 1373 K for 39 h, indicating that these ions were probably reduced to Ti^{2+} [37].

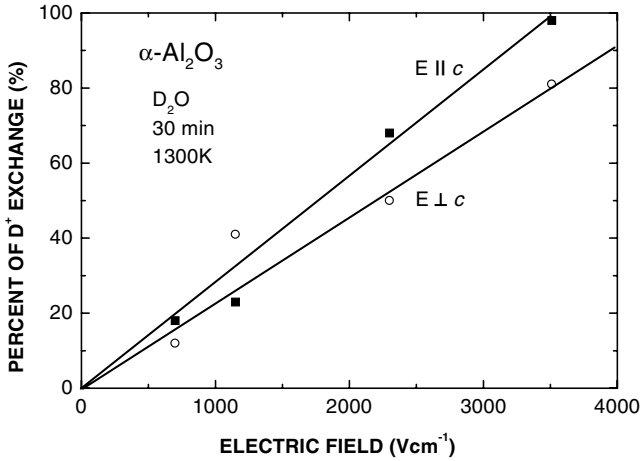

Figure 23. Proton–deuteron exchange (in per cent) against electric field strength at 1300 K. (After [37].)

7. $LiNbO_3$ single crystals

Single crystals of $LiNbO_3$ are being used in many electro-optic and acousto-optic devices [1, 82]. Hydrogen is an important impurity in this material [11, 12, 83–85]. In $LiNbO_3$ crystals, OH^- and OD^- ions absorb at 3480 and 2560 cm^{-1} respectively. The absorption coefficients of the OD^- and OH^- bands depend on the crystal orientation, indicating an anisotropy of the oscillator strength. The band intensity is largest when the *c*-axis of the crystal is oriented parallel to the beam direction [11, 12].

7.1. Thermal diffusion

Hydrogen (deuterium) can be introduced in $LiNbO_3$ by annealing the crystals in $H_2(D_2)$ or $H_2O(D_2O)$ atmospheres at temperatures above 700 K [29, 86–89]. In general, a water vapour atmosphere is preferred because it produces transparent crystals. Anneals in a reducing atmosphere result in dark crystals due to a broad optical absorption band with a peak near 510 nm.

The diffusion coefficients for D^+ were obtained from the growth rate of the absorbance, *A*, of the OD^- bands in three crystals with a thickness of 0.1 cm. The resulting values are: $D_{\|}(923\ \mathrm{K}) = 11 \times 10^{-8}\ \mathrm{cm^2\ s^{-1}}$, $D_{\|}(873\ \mathrm{K}) = 4.5 \times 10^{-8}\ \mathrm{cm^2\ s^{-1}}$ and $D_{\|}(823\ \mathrm{K}) = 2.9 \times 10^{-8}\ \mathrm{cm^2\ s^{-1}}$. In the perpendicular direction, $D_{\perp}(873\ \mathrm{K}) = 5 \times 10^{-8}\ \mathrm{cm^2\ s^{-1}}$ [29]. We conclude that there is no substantial difference in the diffusion coefficients for these two orientations. The activation energy *E* for diffusion parallel to the *c*-axis was obtained using the cross-cut method [57], and the resulting value was 1.4 eV.

7.1.1. Tritium experiments. Experiments with radioactive tritium are difficult and expensive. Very few data are available concerning the infrared characteristics and diffusion properties of tritium in oxides [20, 23, 25, 27, 48, 90–94], in spite of the importance of tritium in advanced energy devices. Here tritium ions were produced by transmutation of ^6Li ions in $LiNbO_3$ single crystals by thermal neutrons [33, 91]. The 'as-grown' crystals exhibited an OH^- vibration band at $\sim$3480 cm^{-1}. After the neutron irradiation, this band was absent and two new bands

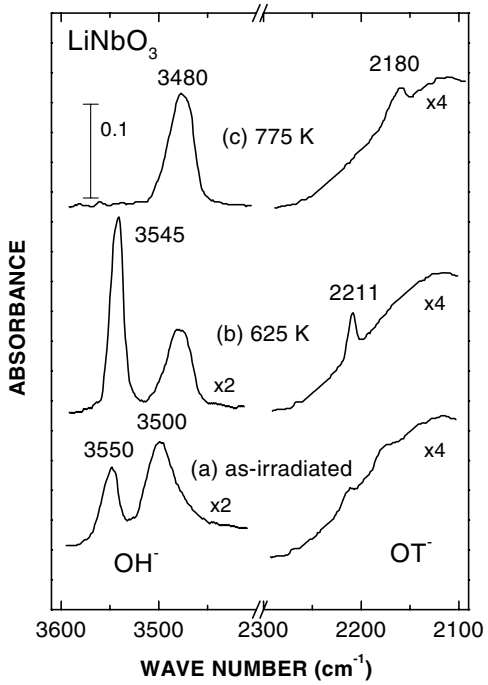

Figure 24. Absorption spectra of a $LiNbO_3$ crystal: bottom, as-irradiated with thermal neutrons ($\approx 7.5 \times 10^{17}$ n cm^{-2}); centre, after subsequent annealing for 1 h at 625 K in air; top, after additional annealing for 1h at 775 K in air. (After [90].)

at 3500 and 3550 cm^{-1} appeared in the OH^- region. In addition, two very weak bands at 2180 and 2211 cm^{-1} were observed (figure 24, bottom) [91]. Following an anneal at 625 K for 1 h, the band at 3500 cm^{-1} was replaced by one at 3480 cm^{-1} (figure 24, centre). The band at 3550 cm^{-1} disappeared and a new band at 3545 cm^{-1} appeared. In the lower-energy region, the band at 2211 cm^{-1} is well resolved and the band at 2180 cm^{-1} has almost disappeared. A subsequent annealing for 1 h at 775 K greatly increased the intensity of the 3480 cm^{-1} band and annihilated that at 3545 cm^{-1} (figure 24, top). Correspondingly, the band at 2211 cm^{-1} disappeared and the band at 2180 cm^{-1} became more prominent [91]. In effect, the top spectrum resembles that of pre-irradiation plus the band at 2180 cm^{-1}.

The frequency ratios between the two OH^- bands at 3545 and 3480 cm^{-1} and their analogues at 2211 and 2180 cm^{-1} are both 1.61, which corresponds well with the theoretical expectation of 1.64. Consequently, we attribute these two bands to OT^- stretching vibrations. The original ^{6}Li concentration in the crystals was $\sim 1.4 \times 10^{21}$ cm^{-3} and the total neutron dose was $\sim 7.5 \times 10^{17}$ n cm^{-2}. Using the cross-section of 910 barns, the resulting tritium concentration was $n(\mathrm{T}) \approx 9.5 \times 10^{17}$ cm^{-3}. The relationship between the tritium concentration and the peak absorption coefficient at 2211 cm^{-1} can be written as

$$n(\mathrm{OT}^-) \approx (1.4 \times 10^{16}\ \mathrm{cm}^{-2})\alpha_{\max}(\mathrm{OT}^-). \tag{9}$$

To compare the out-diffusion of H^+ and T^+, three neutron-irradiated samples with a thickness of 0.1 cm were pre-annealed at 800 K for 1 h in flowing oxygen [33]. After this treatment, only the bands at 3480 and 2180 cm^{-1} were observed, similar to the case shown in figure 24 (top). Subsequently, these crystals were isothermally annealed in flowing oxygen at 900, 930 and 960 K. Using the cross-cut method [57], the resulting activation energies for H^+

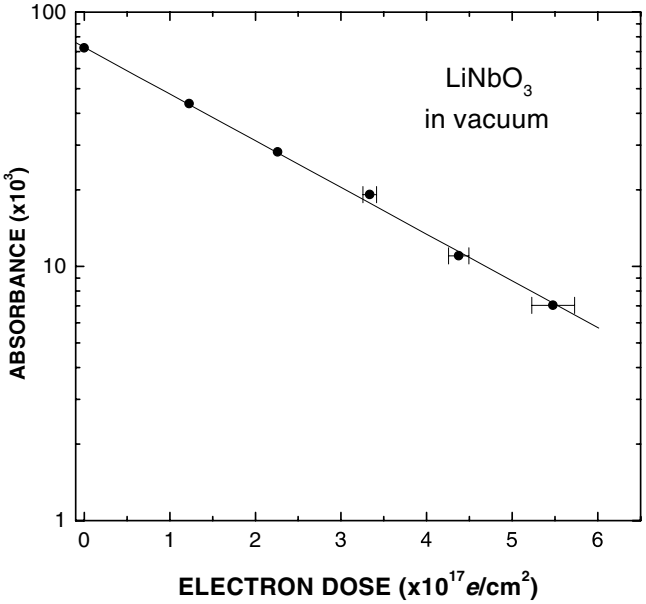

Figure 25. Absorbance of the OD^- band at 2570 cm^{-1} in $LiNbO_3$ versus electron dose at $T \approx 350$ K in a vacuum. (After [36].)

and T^+ out-diffusion were 1.9 ± 0.4 and 1.8 ± 0.4 eV. A semilogarithmic plot of the OH^- absorbances versus isothermal annealing time for the three temperatures using equation (8), yields the diffusion coefficients for hydrogen [33]: $D^{\mathrm{H}}_{out}(900\ \mathrm{K}) = (8 \pm 3) \times 10^{-8}\ \mathrm{cm}^2\ \mathrm{s}^{-1}$, $D^{\mathrm{H}}_{out}(930\ \mathrm{K}) = (12 \pm 5) \times 10^{-8}\ \mathrm{cm}^2\ \mathrm{s}^{-1}$ and $D^{\mathrm{H}}_{out}(960\ \mathrm{K}) = (29 \pm 12) \times 10^{-8}\ \mathrm{cm}^2\ \mathrm{s}^{-1}$. For tritium, the diffusion coefficients are $D^{\mathrm{T}}_{out}(900\ \mathrm{K}) = (12 \pm 6) \times 10^{-8}\ \mathrm{cm}^2\ \mathrm{s}^{-1}$, $D^{\mathrm{T}}_{out}(930\ \mathrm{K}) = (13 \pm 6) \times 10^{-8}\ \mathrm{cm}^2\ \mathrm{s}^{-1}$, and $D^{\mathrm{T}}_{out}(960\ \mathrm{K}) = (24 \pm 12) \times 10^{-8}\ \mathrm{cm}^2\ \mathrm{s}^{-1}$. For these values of diffusion coefficient and thicknesses of about 0.1 cm the condition imposed in section 4, $Dt > 0.005d^2$, is satisfied. These values agree with those found for D^+ in-diffusion from D_2O vapour. Thus, we conclude that there is no significant difference between the diffusion coefficients for the three isotopes.

7.2. Proton/deuteron out-diffusion: effects of environment

The hydrogenic species can be extracted efficiently from $LiNbO_3$ at $T \approx 350$ K by electron irradiation in a vacuum [36]. In contrast, this same effect is not observed when the irradiation is carried out in air. Prior to electron irradiation, the samples were deuterated at 1273 K in flowing D_2O vapour for 30 min. Electron irradiation at $T \approx 350$ K produced a decrease in the OD^- absorption band. In figure 25 the logarithm of the OD^- absorbance at 2570 cm^{-1} is plotted against the electron dose. From the slope we estimate the effective cross-section to be $\approx 10^6$ barns. This enormous cross-section indicates that the displacement of the deuterons is again due to an ionization rather than an elastic collision process. When the same experiment was performed in air [36], in contrast, there was no significant change in the deuteron concentration. These results emphasize the important role played by the surrounding atmosphere. One would surmise that the surfaces serve as a sink for the deuterons, and that the efficiency of out-diffusion should increase with thinner samples.

8. TiO_2 single crystals

The surface of TiO_2 is the most thoroughly studied transition-metal oxide surface owing to its chemisorption and catalytic properties [95]. In the 1970s it was first demonstrated that rutile can be used as a catalytic electrode in a photoelectrolysis cell to decompose water in H_2 and O_2 without the application of external electric field [92]. Photoelectrolysis is still an active area of research in electrochemistry because of the potential of developing passive catalytic generators to produce H_2 as a fuel [95–98].

8.1. Thermal diffusion

The diffusion of hydrogen isotopes in TiO_2 (rutile) has been investigated by several groups [19–22, 24, 25, 30, 48]. Three absorption bands observed at about 3277, 2437 and 2065 cm^{-1} near 300 K have been assigned to OH^-, OD^- and OT^- radicals respectively [48]. The activation energies for diffusion of hydrogen and tritium parallel and perpendicular to the *c*-axis have been determined [22, 25] as $E_{\parallel}(H) = 0.59$ eV, $E_{\parallel}(T) = 0.75$ eV, $E_{\perp}(H) = 1.28$ eV and $E_{\perp}(T) = 1.11$ eV respectively. The diffusion coefficients at 1173 K for protons and tritons can be derived from the Arrhenius equations given in [22] and [25] respectively. The resulting values are $D_{\parallel}(H) = 5.2 \times 10^{-6}$ $cm^2\,s^{-1}$, $D_{\perp} = 1.2 \times 10^{-6}$ $cm^2\,s^{-1}$, $D_{\parallel}(T) = 5.1 \times 10^{-6}$ $cm^2\,s^{-1}$ and $D_{\perp}(T) = 0.3 \times 10^{-6}$ $cm^2\,s^{-1}$.

The activation energies for diffusion of hydrogen and tritium perpendicular to the *c*-axis are much larger than the respective values for diffusion parallel to *c*. This implies that different mechanisms are responsible for the diffusion of hydrogenic species in both directions. Bates and co-workers proposed that diffusion of hydrogen parallel to the *c*-axis proceeds by a proton jump from one O^{2-} ion to another along the channel as represented by $OH^- \cdots O^{2-} \rightarrow O^2 \cdots H^+ \cdots O^{2-} \rightarrow O^{2-} \cdots HO^-$ [24]. They also proposed that diffusion perpendicular to the *c*-axis proceeds by a flipover or rotation of the OH^- bond to move the proton from one channel to an adjacent channel, followed by a proton jump to another O^{2-} ion in the same channel.

8.2. Low-temperature diffusion: channelling effect

The presence of protons in crystalline oxides can sometimes be detrimental for certain applications. A method to remove hydrogenic species at unusually low temperatures, such as near room temperature, has been reported [30]. This method has the important advantage of controlling such diffusion in materials which cannot be subjected to elevated temperatures without structural complications. It involves ionizing radiation by electrons, attended by electric-field sweeping of these species [30].

Rutile has been chosen for demonstration of the feasibility of proton (deuteron) diffusion at low temperatures enhanced by radiation- and electric-field induced diffusion (REID) because it possess a large open channel for easy diffusion [22, 25]. Protons do not thermally diffuse out of TiO_2 below $T \approx 600$ K. The low activation energy for H^+ diffusion along the *c*-axis makes it ideal for such a study. Irradiation was carried out in a deuterated sample with 2.0 MeV electrons. The sample temperature was 340 K and the electric field was 2000 V cm^{-1}. Figure 26(a) shows the spectrum of a $c_{\parallel}$ crystal prior to REID. The crystal contained primarily OD^- and very few OH^- ions. After REID for 1 h, the crystal exhibited the spectrum shown in figure 26(b). Approximately half the deuterons had been swept out and replaced by protons, presumably because of in-diffusion from the electrical contacts and/or atmosphere. After another hour of REID, virtually all the deuterons were removed and replaced by protons, shown in figure 26(c).

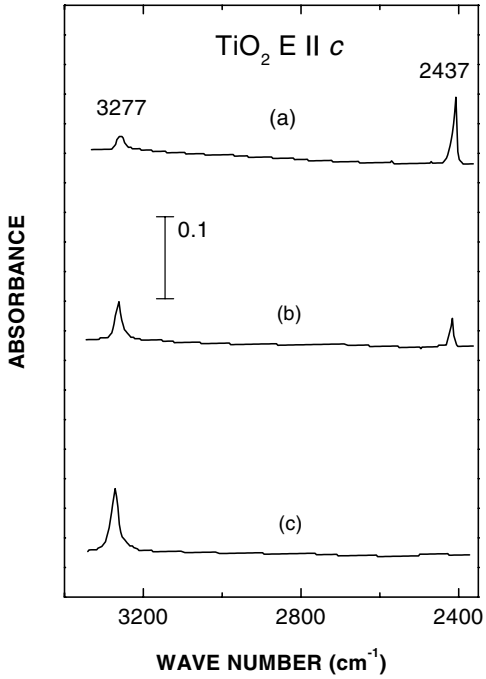

Figure 26. Infrared absorption spectra of a TiO_2 crystal with $E \parallel c$ (a) after deuteration in D_2O for 2 h at 1200 K, and subsequent irradiation with electrons with an applied field of 2000 V cm^{-1} for (b) 1 h and (c) 2 h. (After [30].)

The same experiment was carried out in a $c_\perp$ direction. Some loss of OD^- absorbance was observed, but the out-diffusion rate was less than 5% of that in the $c_\parallel$ direction [30].

REID of deuterons in another $c_\parallel$ sample was performed under identical conditions except the temperature was 390 K [30]. The rate of D^+ removal was twice as fast. There was one other notable difference: the deuterons were not replaced by protons. A profile of the OD^- concentrations was made along the thickness of a crystal after 80% of the deuterons had been removed. Consecutive 0.1 mm increments were removed from the cathode side by polishing. The results showed unambiguously that deuterons were concentrated near the cathode, indicating that the deuterons migrated toward the negative electrode.

The electric field dependence of REID on D^+ out-diffusion was examined in [30]. Several $c_\parallel$ samples were irradiated at 360 K for 30 min each. The results are plotted in figure 27. A strong electric field dependence was observed. Field strengths of less than 1000 V cm^{-1} were not very effective in enhancing D^+ out-diffusion.

9. Concluding remarks

Hydrogenic species normally form thermally stable configurations in oxide crystals near room temperature and diffuse out of the crystal at several hundred degrees above room temperature. The results discussed in the preceding sections unambiguously show that, even at high temperatures, solubilities and diffusion coefficients of hydrogen isotopes in oxides are low compared with those in metals (Pd, Pt, etc). In the bulk the maximum concentration of these isotopes can be estimated to be $\approx 10^{19}$ cm^{-3}. The diffusion coefficients for hydrogen isotopes (in the form of OH^-, OD^- and OT^- radicals) in different oxides are summarized in table 1.

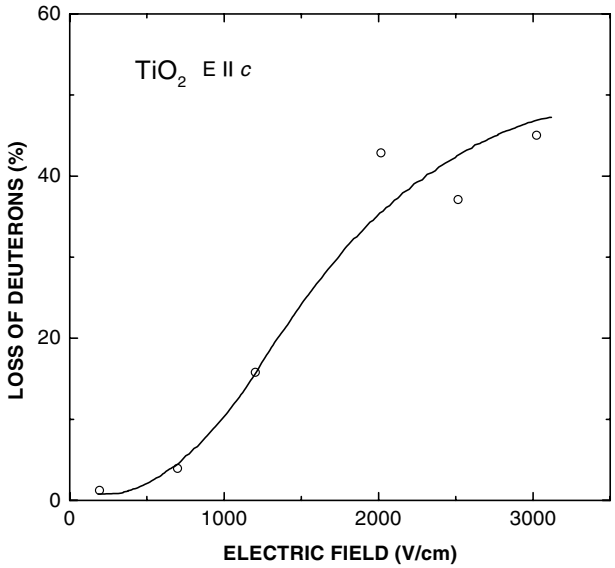

Figure 27. Loss of OD^- absorbance (in per cent) versus electric field strength. Each TiO_2 sample was irradiated for 30 min. (After [30].)

Table 1. Diffusion constants for hydrogen isotopes in some crystalline oxides. The temperatures at which the diffusion coefficients were measured are shown in parentheses.

	MgO (1873 K)	MgO:Li (1173 K)	Al_2O_3 (1273 K)	Al_2O_3:Mg (1273 K)	$LiNbO_3$ (873 K)	$LiTaO_3$[a] (900 K)	TiO_2 (1173 K)	BeO[b] (1273 K)
D ($cm^2\ s^{-1}$)	1.4×10^{-6}	1.0×10^{-6}	1.0×10^{-8} ($\parallel c$)	5×10^{-7}	4.5×10^{-8} ($\parallel c$) 5.0×10^{-8} ($\perp c$)	0.6×10^{-8} ($\parallel c$)	5.2×10^{-6} ($\parallel c$) 1.2×10^{-6} ($\perp c$)	1.1×10^{-11}
E (eV)	—	1.9	5	1.6	1.4	1.5	0.59 $\parallel c$ 1.28 $\perp c$	2.3

[a] Reference [35].
[b] Reference [23].

The largest diffusion coefficients at 1173 K are of the order of 10^{-6} $cm^2\ s^{-1}$, whereas the diffusion coefficient in Pd at the same temperature is 2.9×10^{-4} $cm^2\ s^{-1}$ [99].

The diffusion properties of the hydrogenic isotopes in a given host are governed by three characteristics: (1) the charge or valence, (2) the ionic size and (3) the mass. In principle, some difference in the diffusion coefficient for the three isotopes can be expected. For all practical purposes, the charge and the ionic radii are the same for the three isotopes. However, the mass is different for hydrogen, deuterium and tritium. The results presented in the preceding sections indicate that the charge and/or the ionic size is much more important than the mass in affecting the diffusion behaviour for hydrogen in crystalline oxides with a very different crystalline structure.

Both the dramatic decrease of the threshold temperature for D^+ in-diffusion and the pronounced increase in diffusion coefficients obtained by doping the MgO crystals with lithium concentrations of ≈400 appm are clear indications that some impurities greatly affect the in-diffusion of hydrogen isotopes in MgO. Likewise, enhancement of hydrogen isotope diffusion

has also been observed in Al_2O_3 crystals doped with a magnesium concentration of $\approx$25 appm. We conclude that certain impurities strongly affect the rate of diffusion of hydrogen isotopes in ceramic oxides. From another perspective, Mg is one of the major transmutation products induced in Al_2O_3 crystals by first wall neutrons [16]; thus, production of this impurity by transmutation must be a consideration in the possible use of this material as a deuterium–tritium barrier in fusion reactors.

The diffusion of hydrogenic species depends on crystal orientation for Al_2O_3 and TiO_2 crystals. This dependence is stronger in Al_2O_3 crystals where the in-diffusion of deuterons is 50 times larger in the direction parallel to the *c*-axis. No dependence on crystal orientation was observed in $LiNbO_3$ crystals.

When a moderate electric field is applied the $H^+ \leftrightarrow D^+$ exchange was enhanced in Al_2O_3 crystals. Unlike purely thermal diffusion, an electric field can induce the diffusion of deuterons in as-grown crystals with undetectable OH^- ions. Deuterons can be introduced without an exchange process. This opens up the possibility of proton (deuteron) doping regardless of the initial hydrogen content.

Calculations in conjunction with experimental results indicate that in thermochemically reduced MgO crystals containing $[H^-]^+$ centres the mobile species is not the proton but rather the H^- ion. It is suggested that the mechanism for the diffusion of the hydride ion is a *collinear interstitialcy* mechanism (the interstitial hydride ion hops along the [111] axis and in its saddle point forms a dumbbell with an O^{2-} ion in a regular site) [62].

Under electron irradiation, hydrogenic species become highly unstable at temperatures as low as 85 K; even at this low temperature they are quite mobile. The mechanisms by which the hydrogenic species are displaced from their sites unmistakably involve ionization rather than elastic collisions. The cross-section of 10^8 barns is several orders of magnitude too large to be associated with a knock-on mechanism. A cross-section of this magnitude requires a displacement (or diffusion) mechanism involving capture of secondary electrons and holes created by the primary electrons. The proton, because of its lower mass, is displaced more readily than the deuteron. Whereas the isotopic effect is minimal for thermal diffusion, it is important for RID.

Out-diffusion can be carried out efficiently in rutile near room temperature by breaking the O–H (or O–D) bond during electron irradiation and subsequently sweeping out the protons or deuterons along the *c*-axis by means of an applied electric field. On the basis of this work, it is proposed that diffusion of protons (and perhaps even light impurity ions) can be induced in other oxides with the use of REID. Furthermore, RID of deuterons and tritons has important implications in advanced energy systems.

Acknowledgments

We acknowledge stimulating interaction with M M Abraham, C Ballesteros, I Colera, E A Kotomin, M A Monge, V M Orera, R Pareja, A I Popov, R Ramírez, B Savoini and I Vergara. This research was partially supported by the Comisión Interministerial de Ciencia y Tecnología (CICYT) of Spain.

References

[1] Kaminow I P 1974 *An Introduction to Electro-Optic Devices* (New York: Academic)
[2] Raüber A and Kalchis E (ed) 1978 *Current Topics in Materials Science* vol 1 (Amsterdam: North-Holland) pp 481–601
[3] Gunter P 1982 *Phys. Rep.* **93** 199–299
[4] Narayan J and Chen Y 1984 *Phil. Mag.* A **49** 475–92
[5] Chen Y and González R 1985 *Opt. Lett.* **10** 276–8

[6] Cáceres D, Vergara I, González R and Chen Y 2002 *Phil. Mag.* A **82** 1159–71
[7] Thomas G A, Shraiman B I, Glodis M and Stephen M 2000 *Nature* **404** 262–4
[8] Thomas G A, Ackerman D A, Prucnal P R and Cooper S L 2000 *Phys. Today* **53** 30–6
[9] Van de Walle C G 2000 *Phys. Rev. Lett.* **85** 1012–15
[10] Cox S F J *et al* 2001 *Phys. Rev. Lett.* **86** 2601–4
[11] Cabrera J M, Olivares J, Carrascosa M, Rams J, Müller R and Diéguez E 1996 *Adv. Phys.* **45** 349–92
[12] Wöhlecke M and Kovács L 2001 *Crit. Rev. Solid State Mater. Sci.* **26** 1–86
[13] Clinard F 1984 *J. Mater. Energy Syst.* **6** 100–6
[14] Schiller P 1993 *J. Nucl. Mater.* **206** 113–20
[15] Chen Y *et al* 1994 *J. Nucl. Mater.* **217** 32–47
[16] Rovner L H and Hopkins G R 1976 *Nucl. Technol.* **29** 274–302
[17] Chen Y, Abraham M M and Templeton L C 1977 *J. Am. Ceram. Soc.* **60** 101–4
[18] Chen Y and González R 1993 *Trans. Mater. Res. Soc. Japan* B **19** 1043–56
[19] de Ford J W and Johnson O W 1973 *J. Appl. Phys.* **44** 3001–7
[20] Johnson O W, de Ford J W and Shaner J W 1973 *J. Appl. Phys.* **44** 3008–12
[21] de Ford J W and Johnson O W 1975 *J. Appl. Phys.* **46** 1013–22
[22] Johnson O W, Paek S H and de Ford J W 1975 *J. Appl. Phys.* **46** 1026–33
[23] Fowler J D, Chandra D, Elleman T S, Payne A W and Verghese K 1977 *J. Am. Ceram. Soc.* **60** 155–61
[24] Bates J B, Wang J C and Perkins R A 1979 *Phys. Rev.* B **19** 4130–9
[25] Cathcart J V, Perkins R A, Bates J B and Manley L C 1979 *J. Appl. Phys.* **50** 4110–19
[26] Engstrom H, Bates J B, Wang J C and Abraham M M 1980 *Phys. Rev.* B **21** 1520–6
[27] Engstrom H, Bates J B and Boatner L A 1980 *J. Chem. Phys.* **73** 1073–7
[28] González R, Chen Y and Tsang K L 1982 *Phys. Rev.* B **26** 4637–45
[29] González R, Chen Y, Tsang K L and Summers G P 1982 *Appl. Phys. Lett.* **41** 739–41
[30] Chen Y, González R and Tsang K L 1984 *Phys. Rev. Lett.* **53** 1077–9
[31] González R and Chen Y 1987 *Phys. Rev.* B **35** 8202–6
[32] González R, Chen Y, Barhorst J F and Tsang K L 1987 *J. Mater. Res.* **2** 77–81
[33] González R, Ballesteros C, Chen Y and Abraham M M 1989 *Phys. Rev.* B **39** 11085–92
[34] Park J L and González R 1989 *J. Mater. Res.* **4** 224–31
[35] González R, Hantehzadeh R, Chen C Y, Halliburton L E and Chen Y 1989 *Phys. Rev.* B **39** 1302–6
[36] González R, Hodgson E R, Ballesteros C and Chen Y 1991 *Phys. Rev. Lett.* **67** 2057–9
[37] Ramírez R, González R, Colera I and Chen Y 1997 *Phys. Rev.* B **55** 237–42
[38] Ramírez R, González R, Colera I and Vila R 1997 *J. Am. Ceram. Soc.* **80** 847–50
[39] Chen Y, Abraham M M and Tohver H T 1976 *Phys. Rev. Lett.* **26** 1757–60
[40] Chen Y, González R, Schow O E and Summers G P 1983 *Phys. Rev.* B **27** 1276–82
[41] Briggs A 1975 *J. Mater. Sci.* **10** 729–36
[42] Corisco M S, González R and Ballesteros C 1985 *Phil. Mag.* A **52** 699–711
[43] González R, Chen Y and Mostoller M 1981 *Phys. Rev.* B **24** 6862–9
[44] Herrington J R, Dischler B, Räuber A and Schneider J 1973 *Solid State Commun.* **12** 351–4
[45] Kovács L, Szalay V and Capelletti R 1984 *Solid State Commun.* **52** 1029–31
[46] Kovács L, Szaller Z S, Cravero I, Földvári I and Zaldo C 1990 *J. Phys. Chem. Solids* **51** 417–20
[47] Kovács L, Wöhlecke M, Jovanovic A, Polgár K and Kapphan S 1991 *J. Phys. Chem. Solids* **52** 797–803
[48] Bates J B and Perkins R A 1977 *Phys. Rev.* B **16** 3713–22
[49] Andersson P O, Kollberg E L and Jelenski A 1973 *Phys. Rev.* B **8** 4956–65
[50] Tollestrup A, Fowler W A and Lauritsen C C 1950 *Phys. Rev.* **78** 372–4
[51] Crank J 1956 *The Mathematics of Diffusion* (Oxford: Clarendon)
[52] Abraham M M, Butler C T and Chen Y 1971 *J. Chem. Phys.* **55** 3752–6
[53] Volkl J and Alefeld G 1978 *Hydrogen in Metals* vol 1, ed G Alefeld and J Volkl (Berlin: Springer)
[54] Gorham-Borgeron E 1976 *Phys. Rev. Lett.* **37** 146–50
[55] Stoneham A M 1978 *J. Nucl. Mater.* **69–70** 109–16
[56] Chen Y, Montesa E, Boldú J L and Abraham M M 1981 *Phys. Rev.* **24** 5–10
[57] Damask A C and Dienes G J 1963 *Point Defects in Metals* (New York: Gordon and Breach)
[58] Doherty S P, Martin J J, Armington A F and Brown R N 1980 *J. Appl. Phys.* **51** 4164–8
[59] Chen Y, Abraham M M, Templeton L C and Unruh W P 1975 *Phys. Rev.* B **11** 881–90
[60] Jeffries B T, González R, Chen Y and Summers G P 1982 *Phys. Rev.* B **25** 2077–80
[61] González R, Pareja R and Chen Y 1992 *Phys. Rev.* B **45** 12730–5
[62] Monge M A, González R, Popov A I, Pareja R, Chen Y, Kotomin E A and Kuklja M M 1999 *Defect and Diffusion Forum* **169–170** 1–11

[63] Kuklja M M, Stefanovich E V, Kotomin E A, Popov A I, González R and Chen Y 1999 *Phys. Rev.* B **59** 1885–90
[64] Puchin V E, Shluger A L and Itoh N 1995 *Phys. Rev.* B **52** 6254–64
[65] Puchin V E, Tanimura K and Itoh N 1993 *Phys. Rev.* B **47** 6226–40
[66] Pandey R and Vail J M 1989 *J. Phys.: Condens. Matter* **1** 2801–20
[67] Vail J M 1990 *J. Phys. Chem. Solids* **51** 589–607
[68] Wang Q S and Holzwarth N A W 1990 *Phys. Rev.* B **41** 3211–25
[69] Sibley W A and Chen Y 1967 *Phys. Rev.* **160** 712–16
[70] Wang H A, Lee C H, Kroger F A and Cox R T 1983 *Phys. Rev.* B **27** 3821–41
[71] Paladino A E and Kingery W D 1962 *J. Chem. Phys.* **37** 957–62
[72] Mohapatra S K and Kroger F A 1977 *J. Am. Ceram. Soc.* **60** 141–8
[73] Vila R and Jiménez de Castro M 1994 *Phys. Rev.* B **49** 1696–704
[74] Cox R T 1971 *Solid State Commun.* **9** 1989–92
[75] Schirmer O F 1971 *J. Phys. Chem. Solids* **32** 499–509
[76] Abraham M M, Unruh W P and Chen Y 1974 *Phys. Rev.* B **10** 3540–5
[77] Abraham M M, Chen Y, Boatner L A and Reynolds R W 1976 *Phys. Rev. Lett.* **37** 849–52
[78] Ramírez R, González R, Pareja R and Chen Y 1997 *Phys. Rev.* B **55** 2413–16
[79] Tardío M M, Ramírez R, González R and Chen Y 2001 *Appl. Phys. Lett.* **79** 206–8
[80] Zinkle S J and Kinoshita C 1997 *J. Nucl. Mater.* **251** 200–17
[81] Oishi Y, Ando K, Suga N and Kingery W D 1983 *J. Am. Ceram. Soc.* **66** C130–1
[82] Lines M E and Glass A M 1977 *Principles and Applications of Ferroelectrics and Related Materials* (Oxford: Oxford University Press)
[83] Smith R G, Fraser D B, Denton R T and Rich T C 1968 *J. Appl. Phys.* **39** 4600–2
[84] Vormann H, Weber G, Kapphan S and Kratzig E 1981 *Solid State Commun.* **40** 543–5
[85] Fowler W B, Capelleti R and Colombi E 1991 *Phys. Rev.* B **44** 2961–8
[86] Bollmann W and Gernard M 1972 *Phys. Status Solidi* a **9** 301–8
[87] Bollmann W and Stöhr H L 1977 *Phys. Status Solidi* a **39** 477–84
[88] Ketchum J L, Sweeney K L, Halliburton L E and Armington A F 1983 *Phys. Lett.* A **94** 450–3
[89] De Rosendo M J, Arizmendi L, Cabrera J M and Agulló-Lopéz F 1986 *Solid State Commun.* **49** 499–501
[90] Tanifuji T, Noda K, Takahashi T and Watanabe H 1987 *J. Nucl. Mater.* **149** 227–32
[91] González R, Chen Y and Abraham M M 1989 *Phys. Rev.* B **37** 6433–5
[92] Shluger A, Itoh N and Noda K 1991 *J. Phys.: Condens. Matter* **3** 9895–906
[93] Shah R, De Vita A and Payne M C 1995 *J. Phys.: Condens. Matter* **7** 6981–92
[94] Shah R, De Vita A, Heine V and Payne M C 1995 *Phys. Rev.* B **53** 8257–61
[95] Henrich V E and Cox P A 1994 *The Surface Science of Metal Oxides* (Cambridge: Cambridge University Press)
[96] Fujishima A and Honda K 1972 *Nature* **238** 37–8
[97] Hill G J 1968 *Br. J. Appl. Phys. (J. Phys. D)* **1** 1151–62
[98] Linsebigler A L, Lu G and Yates J T Jr 1995 *Chem. Rev.* **95** 735–58
[99] Scott J L 1978 *Met. Prog.* **114** 40–9